Fundamental Understanding of the Interactions between Elemental Selenium and Hydrophilic/Hydrophobic Particles in Wastewater

by

Junmeng Li

A thesis submitted in partial fulfillment of the requirements for the degree of

Master of Science

in

Chemical Engineering

Department of Chemical and Materials Engineering

University of Alberta

Abstract

In this study, interactions between elemental selenium particles and different surfaces (i.e. $Fe(OH)_3$, silica, octadecyltrichlorosilane (OTS) modified silica and selenium film coated gold) are investigated to understand the behavior of elemental selenium particles in wastewater treatment process. It is found that the Derjaguin-Landau-Verwey-Overbeek (DLVO) forces govern the attachment of elemental selenium particle to $Fe(OH)_3$ and silica surfaces, while additional attractive hydrophobic forces are found when elemental selenium particles interact with OTS modified surface and selenium film. However, elemental selenium is less hydrophobic in nature than OTS modified surface. When $Fe(OH)_3$ is used as a coagulant, the salt concentration greatly impacts the $Fe(OH)_3$ morphology and the interacting forces that the polymer behavior of $Fe(OH)_3$ is promoted at low salt concentration. And the electric double layer (EDL) force decreased and the Van der Waals force dominates at high salt concentration. The fundamental understanding of the interactions between selenium and hydrophobic/ hydrophilic particles in wastewater accelerates the development of new technology for the removal of selenium from industry wastewater.

Preface

Chapter three of this thesis will be sent for publication to the *Environmental Science and Pollution Research* journal as Junmeng, L., Jingyi, W., Liu, Q., and Zeng, H., "Understanding the mechanism of interactions between elemental selenium and ferric hydroxide in wastewater". I was responsible for the data collection and analysis as well as the manuscript composition. Jingyi, W. assisted the data collection and contributed to manuscript edits. Liu, Q. and Zeng, H., were the supervisory authors and were involving with concept formation and manuscript composition.

Chapter four of this thesis will be sent for publication to the *Langmuir* journal as Jingyi, W., Junmeng, L., Liu, Q., and Zeng, H., "Investigation of interactions between elemental selenium and hydrophilic/hydrophobic surface: direct force measurement using AFM". Jingyi, W. and I was responsible for the data collection and analysis as well as the manuscript composition. Liu, Q. and Zeng, H., were the supervisory authors and were involving with concept formation and manuscript composition.

Part of the Chapter three and four of this thesis was presented at the C^5MPT student seminar as "Fundamental understanding of the interactions between elemental selenium and hydrophilic/hydrophobic surfaces".

Acknowledgment

I would like to give my sincere gratitude and appreciation to:

- My supervisors, Dr. Qingxia (Chad) Liu and Dr. Hongbo Zeng for their kind guidance and great support throughout my master degree study.
- Dr. Jingyi Wang for her great help on AFM measurement training, experiment design and advice on many details of my work.
- Ms. Patricia Siferd, Mr. Carl Corbett and Ms. Lily Laser for always being very accommodating.
- My colleagues, You Fu, Chen Shi, Lei Xie, Xin Cui, Wenda Xiao, Mingbo Zhang, Li Xiang, Shuo Zhang, Jing Liu, Dr. Bing Yan, Han Lu, Jiawen Zhang, Yuxi Liu and all the other group members. Without all of you, I could not get this far.
- Dr. Guangcheng Chen from Department of Earth & Atmospheric Sciences for ICP-MS experiment and analysis services.
- Natural Sciences and Engineering Research Council of Canada (NSERC), Teck Metals Ltd., Canada Foundation for Innovation (CFI) and Canadian Centre for Clean Coal/ Carbon and Mineral Processing Technologies (C^5MPT) for financial support.

Finally, to my family for supporting me from the very beginning of my study.

Table of Contents

List of Tables

List of Figures

List of Symbols

A	Hamaker constant

Au	Gold
D	Separation distances
ε_0	vacuum permittivity
F	Intermolecular forces
F_{edl}	Electric double layer force
F_{vdw}	Van der Waals force
Δm	Mass change of sensor
ΔD	Dissipation change of sensor
κ	Debye length
n	Resonance number of sensor
R	Selenium probe radius
T	Temperature
σ_T	Tip surface charge density
σ_s	Substrate surface charge density
ψ_0	Surface charge potential
ψ_T	Tip potential
ψ_S	Substrate potential

List of Abbreviations

AFM	Atomic force microscope

DLVO theory	Theory developed by Derjaguin, Landau, Verwey and Overbeek
EDL	Electric double layer
FBR	Fluidized bed reactor
ICP-MS	Inductively coupled plasma mass spectrometry
OTS	Octadecyltrichlorosilane
ppm	Parts per million
ppb	Parts per billion
PB equation	Poisson-Boltzmann equation
QCM-D	Quartz crystal microbalance with dissipation monitoring
VDW	Van der Waals
WHO	World Health Organization
ZVI	Zero valent iron

Chapter 1 Introduction

1.1 Background of selenium pollution

Selenium (Se) is a necessary nutrient element for life in trace amount, but both excess and deficient diet intake of Se could cause severe damage to human and animal body (Foster & Sumar, 1997). World Health Organization (WHO) has proposed a guideline value of 40 μg/day with maximum intake of 400 μg/day (WHO, 2011). By consuming sufficient amount, it has been studied that Se plays significant roles on several major metabolic pathways such as antioxidant defense system and immune function (Brown & Arthur, 2001). However, Keshanin-Beck disease, a disease of the bone, was reported to be caused by extremely low level of Se in soil in areas of northern China and eastern Siberia (Foster & Sumar, 1997). In contrast, many cases have been investigated due to high level of selenium which causes reproductive failures/abnormalities in aquatic vertebrates (i.e., fish, bird and reptiles) (Brown & Arthur, 2001; Frankenberger & Engberg, 1998).

Although the highest selenium concentrations are found in rocks such as black shales (around 600 ppm) and phosphate rocks (300 ppm) (Haygarth, 1994), the human processes have driven the migration of selenium to soil, water and atmosphere. As can be seen form Fig. 1.1, a global pathway for selenium suggests that human (anthropogenic) actions can redistribute selenium resource and increase the selenium level through activities such as mining operation, refinery process, fossil fuel combustion and agriculture drainage which cause serious selenium pollution to the environment.

Figure 1.1. Global cycling pathway for Se. (Source: adapted from Haygarth, 1994)

1.2 Selenium aquatic chemistry

Among all the pathways of selenium pollution, those on earth surface (terrestrial) especially in aquatic environment are considered as the major causes to animal toxicity by dietary intake (Foster & Sumar, 1997). A water chemistry of selenium is shown in Fig. 1.2. When the selenium wastewater is disposed to the aquatic environment, selenium is taken up by phytoplankton, zooplankton and other aquatic vertebrates. San Joaquin Valley and Elk river valley (Sobolewski, 2005), for example, were reported that selenium levels were elevated in birds and fish body.

The aquatic chemistry of selenium can be very complicated as it could have four different oxidation states and many organic forms as can be seen in Table 1.1. Furthermore oxyanions, selenite (SeO_3^{2-}) and selenate (SeO_4^{2-}) in wastewater are the predominate forms

and mostly contribute to selenium pollution in aquatic environment (Kapoor, Tanjore, & Viraraghavan, 1995; Lemly, 2004). The elemental selenium (Se^0), in comparison with SeO_3^{2-} and SeO_4^{2-}, has much less toxic effect (H. Wang, Zhang, & Yu, 2007), which makes the reduction of Se oxyanions to elemental selenium a promising approach for Se removal from aqueous system.

Figure 1.2. Water chemistry of selenium. (Source: adapted from Burau (1985))

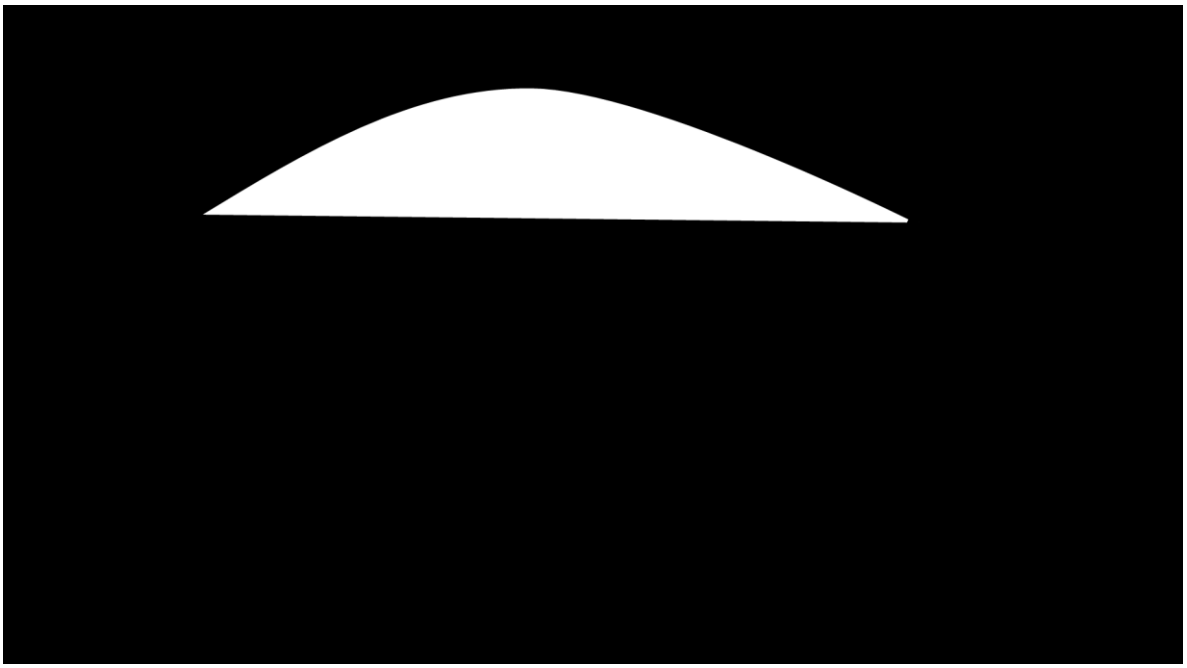

Table 1.1. Chemical state of selenium in aquatic environment

States	Forms
Se^{2-} (Selenide)	HSe^-, H_2Se
Elemental Se	Se^0
Se^{4+}(Selenite)	SeO_3^{2-}, $HSeO_3^-$, H_2SeO_3
Se^{6+}(Selenate)	SeO_4^{2-}, $HSeO_4^-$, H_2SeO_4
Organic Selenium	Selenomethionine, Selenocysteine…

1.3 Selenium removal technologies

According to the review reports from North American Metals Council Selenium Working Group (NAMC-SWG), major available technologies for removing selenium are categorized into three parts as shown in Table 1.2 (Sandy & DiSante, 2010). Several challenges are found when demonstrating selenium removal process: 1. selenium is usually dilute in solution and need to meet requirement of 5 ppb; 2. it exists in different chemical forms that needs technologies to remove the selenite and selenate.

Table 1.2. Major technologies available for selenium removal.

Physical	Chemical	Biological
Reverse Osmosis	Zero valent iron	Bioreactor
	Co-precipitation	Passive treatment
	Adsorption	

1.3.1 Physical treatment

In reverse osmosis process, wastewater is forced into membrane to overcome osmotic pressure and purified by remaining the impurities such as sand particles, and salt ions. It has been successfully applied to desalination industry (Fritzmann, Löwenberg, Wintgens, & Melin, 2007). A pilot study has been demonstrated at a phosphate mine plant through low pressure reverse osmosis in Idaho, where the effluent selenium concentration could be as low as 1 ppb. However, there is no commercial plant that has applied this technique and it also requires extensive pretreatment of mine waters to remove solids and to lower the concentration of total dissolved solids for avoiding fouling in the membrane (Twidwell, McCloskey, Miranda, & Gale, 2000).

1.3.2 Chemical treatment

The chemical treatment methods rely on the reactivity of selenium with the selected reagent. Zero valent iron (ZVI) was used to reduce selenite and selenite to elemental form. The general mechanism can be described as Equation (1.1) and (1.2).

$$3Fe^0(solid)+SeO_4{}^{2-}+8H^+ \rightarrow 3Fe^{2+}+Se^0+4H_2O \quad (1.1)$$

$$2Fe^0(solid)+SeO_3{}^{2-}+6H^+ \rightarrow 2Fe^{2+}+Se^0+3H_2O \quad (1.2)$$

The product of elemental selenium is insoluble in solution and can be removed by the ferrous or ferric products, where the elemental selenium particles are enmeshed into ferric or ferrous precipitates. Furthermore the by-product $Fe(OH)_2$ (green rust) can promote the reduction of selenate to selenite (Zhang, Wang, Amrhein, & Frankenberger, 2005). Pilot, bench and full scales tests for selenium removal studies have successfully conducted on

coal mining wastewater process and flue gas desulfurization (FGD) units but a further treatment is needed as a large amount of iron precipitates are produced (Hill, 2010).

Co-precipitation process is used mainly to adsorb selenite on ferric oxyhydroxide as described in Equation (1.3) (Hill, 2010):

$$SeO_3^{2-} + FeCl_3 + 3H_2O \rightarrow Fe(OH)_3 \cdot SeO_3^{2-} + 3H^+ + 3Cl^- \quad (1.3)$$

90% of selenite removal has reported with effective pH range of 5 to 8 (Balistrieri & Chao, 1990). Therefore, co-precipitation would be applicable for selenite rich wastewater or processes that reduce selenate first.

Adsorption process offers very flexible design parameters as there are a large number of adsorbents available for selenium removal. Various materials, including fly ash, and other surface reactivate adsorbents such as activated carbon, activated aluminum oxide and mesoporous materials have been widely used in wastewater treatment (Fu, 2014).

1.3.3 Biological treatment

In order to reduce selenium oxyanions to elemental selenium, biological reduction technologies have been studied comprehensively and proved to be industrially feasible (Hill, 2010; Munirathinam, Srinivasan, Tudini, Sandy, & Harrison, 2011). Specifically fluidized bed reactor (FBR) and ABMet® technologies both have been conducted on pilot and full scale for treating mining and coal fire power plant wastewater (Fitzpatrick, 2013; Hatzinger et al., 2000; Sonstegard, Pickett, Harwood, & Johnson, 2008). Several advantages are offered by FBR: good contact can be achieved resulting in high removal efficiency; biofilm thickness can be controlled; and clogging and channeling can be

avoided in this process. A large amount of energy is required to maintain sufficient high velocity up flow through bed (Bitton, 2005). A typical one stage FBR unit is shown in Fig. 1.3. Major units consist of heating system, fluidized pump, fluidized bed vessel and ballasted sand clarifier. The feed waste water first enters the heating system to main a minimum temperature around 10 ℃. This ensures bacteria to be biological active for reducing selenite and selenate. After going through the heating system, the electron donor, macronutrient and trace nutrient are injected inline. Then the effluent is delivered to FBR by fluidized pump that generate enough flow velocity for FBR reaction. There is also a recycle line coming from top of FBR to the suction side of fluidized pump. Fluidized bed column is the core part of FBR unit where selenium oxyanion reduction is taking place. With enough flow rates provided by fluidized pump, small particle media (e.g., Microsand) is suspended to around two third of height of reactor column. The suspend bed provides large surface areas for microbes growth and full contact of waste water with microbes. The microbes are heterotrophic cultural to maintain efficient reducing performance. One group of bacteria usually reduces selenate to selenite and another type reduces selenite to elemental selenium. There are wide ranges of selection bacteria available in nature, but reports have suggested using local microorganism from the work plant area (Webster, Guarini, & Wong, 2009). However biogenerated elemental selenium are stable colloidal properties in bulk solution that are usually in size of 50 to 500 nm and highly negatively charged (i.e., around - 40 mV) at natural pH (i.e., pH 6.0 – 8.0); therefore, particle removal by gravity settling could not be applied in this case (Buchs, Evangelou, Winkel, & Lenz, 2013). Coagulation and flocculation processes are needed as a tertiary treatment before the secondary FBR process, for removing selenium particles. As can be seen from the figure,

a ballasted sand clarifier is applied for this case. The major components of ballasted sand clarifier consist of two or three mixing tanks, a lamellar settler and a hydrocyclone. Ferric chloride and polymer are injected in mixing tanks to produce coagulants and flocculants with the help of agitator providing more collision opportunities and larger contact area.

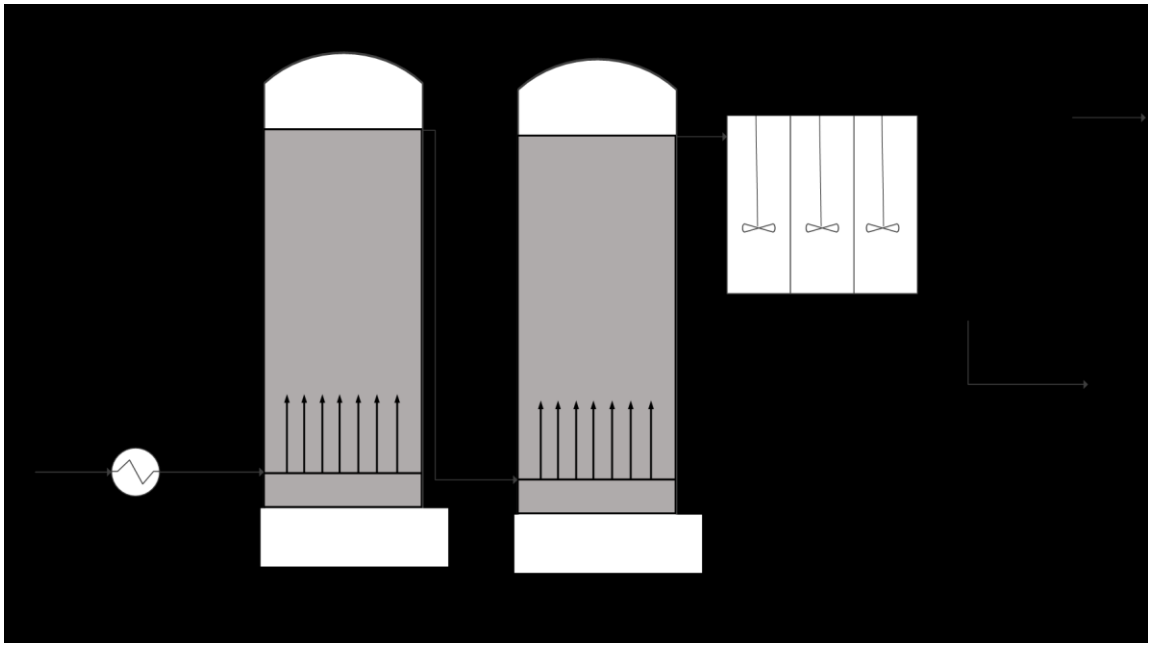

Figure 1.3. Schematic diagram of FBR system process

1.4 Intermolecular and surface forces

In order to understand the behavior of elemental selenium in wastewater, the most direct way is to investigate the intermolecular forces acting between elemental selenium and different particles, which are of great significance to understand the coagulation mechanism at micro and even nano levels.

1.4.1 Van der Waals (VDW) force

Van der Waals (VDW) force, named after Dutch scientist Johannes Diderik van der Waals, is to describe the force between atoms and/or molecules by summing of three different forces which are orientation/Keeson force, induction/Debye force, and dispersion/London force (Cappella & Dietler, 1999). It is a weak force compared to hydrogen bonding, and coulombic interaction, but it plays significant role for understanding phenomena such as adhesion, surface tension, and wetting. VDW force is believed to exist between all atoms and molecules in contrast to the other kinds of forces that may not exist under certain conditions. VDW force is a long range force that can be effective from 10 nm to 0.2 nm. However VDW force is not generally pairwise additive as the force between two particles molecules is also affected by other molecules nearby. Therefore, VDW interactions depend on the geometries of interacting surfaces. In this project a sphere-surface model is used and expressed as Equation (1.4). (J. N. Israelachvili, 2011).

$$F_{\mathrm{vdw}} = -\frac{AR}{6D^2} \tag{1.4}$$

where A is the Hamaker constant in bulk media, which is defined as $A = \pi^2 C_{VDW} \rho_1 \rho_2$, C_{VDW} is a constant depending on the optical properties and geometry of the interacting bodies and ρ_1 and ρ_2 are the numbers of atoms per unit volume in the two bodies, R is the sphere radius, and D is the separation distance.

1.4.2 Electric double layer (EDL) force

VDW forces alone only determine the interactions in relatively simple system such as vacuum or nonpolar wetting film. In more complex system , such as colloidal particle, the surface of particle are charged in bulk solution media, which give arise to electrostatic forces known as electric double layer (EDL) force. It is also of fundamental importance to the stability of colloidal particle in liquid. The surface charging of a particle can be from many ways including (1) ionization or dissociation of surface groups (e.g., $COOH \rightarrow COO^- + H^+$); (2) adsorption of ions from the solution (e.g., adsorption of cations Ca^{2+} to anionic – COO^- sites on the surface); and (3) substitution of surface ions (J. N. Israelachvili, 2011). A schematic diagram of EDL is shown in Fig. 2.2 in Experimental Techniques section. The particle carries positive or negative charges. Taking negatively charged particle as an example, the positive charged ions, namely counterions, are accumulated near the particle surface. The first layer where counter-ions are adsorbed and boned to the charged particle surface is so-called Stern layer, at which the electric potential decreases linearly as the distance increases. The second layer is called diffusive layer where both counterions and co-ions exist. And the distribution of counterions can be described by Poisson-Boltzmann (PB) Equation as:

$$\frac{d^2\psi}{dx^2} = -\frac{ze\rho}{\varepsilon_0\varepsilon} = -\frac{ze\rho_0}{\varepsilon_0\varepsilon}e^{-\frac{ze\psi}{kT}} \tag{1.5}$$

where ψ is the electrostatic potential, x is the gap between the ion and surface, ρ is the counter ion density, z is the valency of the ion, ε_0 and ε are the permittivity of vacuum and dielectric constant respectively, k is the Boltzmann constant and T is the absolute temperature.

And the charge density of the ions in solution is governed by Grahame Equation:

$$\sigma = \left\{ 2\varepsilon_0 \varepsilon kT \left(\sum_i \rho_{0i} - \sum_i \rho_{\infty i} \right) \right\}^{\frac{1}{2}} \tag{1.6}$$

In this project, the EDL force equation of (1.7) is used for the case of a sphere approaching to an infinite flat substrate:

$$F_{\text{edl}} = \frac{\pi}{\varepsilon\varepsilon_0 {\kappa_D}^2} [({\sigma_T}^2 + {\sigma_s}^2)(\mathrm{e}^{-2\kappa_D R} + 2K_D R - 1)\mathrm{e}^{-2\kappa_D D} + 4\sigma_T \sigma_s (\mathrm{e}^{-\kappa_D R} + \kappa_D R - 1)\mathrm{e}^{-\kappa_D R}] \tag{1.7}$$

where σ_{T} is the tip surface charge density, σ_{s} is the substrate surface charge density and κ is the Debye length. Equation (1.7) assumed the surface charges of particles are constants as the surface potentials of the materials used in this project are pH dependent. Therefore, the constant charge EDL equation could better reveals the interactions between particles.

1.4.3 Non-DLVO forces: Hydrophobic force

Attractive forces between hydrophobic particles in water have been investigated in different systems as it cannot be accounted for the attractive VDW force. Hydrophobic particles, such as saturated hydrocarbons have low solubility in water and tend to aggregate in solution. The origin of hydrophobic force is not well understood, but several hypotheses have been proposed (Cappella & Dietler, 1999):

1. Hydrophobic force could originate from changes of the water structure in the thin water layer between hydrophobic surfaces compared to that in bulk water.
2. It could be the capillary force due to cavitation in the vicinity of hydrophobic surfaces.

3. And it could be originated from hydrodynamic fluctuation at a hydrophobic surface/water interface.

Since there is no theory to describe hydrophobic forces, an empirical model is used (Meyer, Rosenberg, & Israelachvili, 2006; Rabinovich & Yoon, 1994) to theoretically describe the hydrophobic force profile from AFM force measurement:

$$F = C_1\, exp\left(-\frac{D}{D_1}\right) + C_2 exp(-\frac{D}{D_2}) \tag{1.8}$$

where C_1 and C_2 are the strength of the short and long range force respectively, and D_1 and D_2 are the respective decay lengths. The short rang hydrophobic attraction is in the range from 1 to 2 nm.

1.5 Objectives and scope

After selenium particles produced from FBR process, the wastewater is pumped to the clarifier as described in Fig. 1.3 where settling takes place. In order to understand how elemental selenium behaves in settling process, four different kinds of particles need to be considered, which are sands mostly in silica content, hydrophobic particles as polymer coated sand particles, elemental selenium from FBR process and $Fe(OH)_3$ for selenium removal. Therefore, four different particles interactions have to be investigated that are selenium-silica, selenium-hydrophobic particles, selenium-selenium and selenium-$Fe(OH)_3$ interactions as can be seen in Fig. 1.4. AFM force, zetapotential and QCM-D measurement are conducted to mimic such interactions. And settling experiments and ICP-MS measurements are used to determine the removal efficiency under different conditions (i.e. pH and dosage). The overall objectives of this project are: first finding out the best

removal conditions for selenium removal using specific coagulant or flocculation; second fundamentally understand the elemental form selenium behavior in wastewater which both provide guidance for wastewater treatment industry.

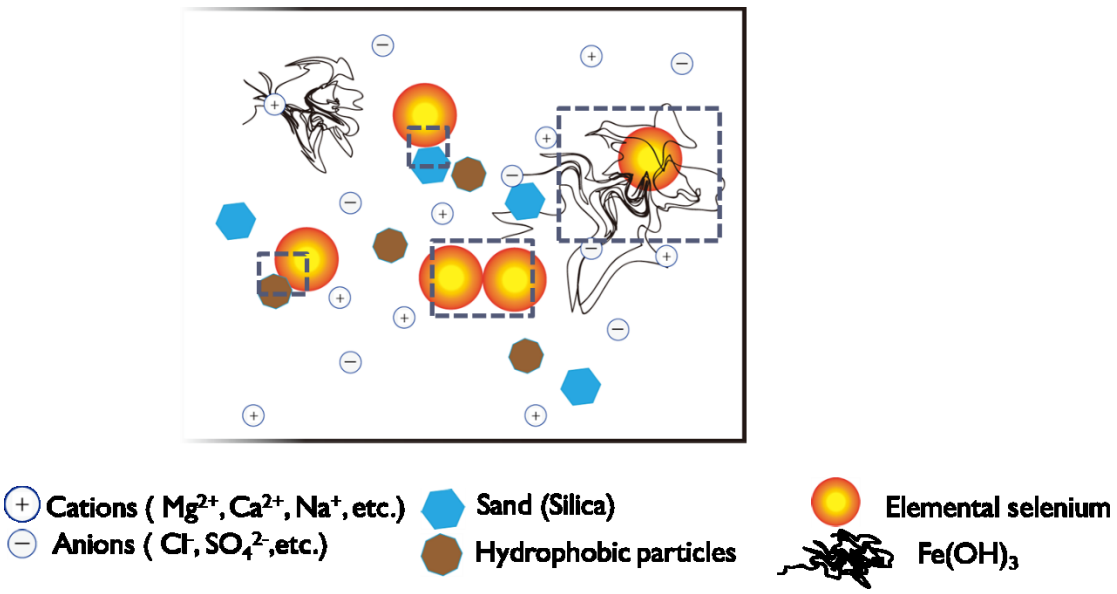

Figure 1.4. Schematic diagram of possible interactions between elemental selenium particles and impurities in wastewater.

1.6 Outline of this thesis

The background of selenium pollution, challenges, water chemistry, and selenium removal methods are introduced in this chapter.

Chapter two describes the techniques and equipment for understanding the interactions between elemental selenium and hydrophobic or hydrophilic surface and determining the efficient pH conditions for selenium removal in wastewater.

The pH efficiency of SeNPS removal and mechanism of interactions between SeNPs and $Fe(OH)_3$ were investigated in chapter three. The settling condition for the wastewater

studies is suggested at around pH 8 which SeNPs are settled due to sweep flocculation and trapped by $Fe(OH)_3$ polymer that is favor for later sludge treatment process. The interactions between SeNPs and $Fe(OH)_3$ in wastewater are governed by Van der Waals force since the EDL force are depressed at high salt concentration. Polymer behaved $Fe(OH)_3$ at boundary of the surface could facilitate the SeNPs adsorption and the morphology of $Fe(OH)_3$ is impacted by the salt concentration.

Chapter four discuss the AFM force measurements between elemental selenium particles with hydrophilic or hydrophobic surfaces under different pH and salt conditions to better how SeNPs interact with different particles. In short, when selenium particles interact with hydrophilic surfaces Van der Waals force dominates at high salt concentration and DLVO force dominates at low salt concentration. When selenium particles interact with hydrophobic surfaces Van der Waals with hydrophobic forces dominate at high salt concentration and DLVO with hydrophobic forces dominate at low salt concentration. It is also found that selenium is less hydrophobic than OTS from adhesion and contact angle results.

Chapter five summarizes the major findings and results which provides better understanding of the coagulation process mechanism for treating selenium polluted wastewater.

Chapter six suggests future works including AFM forces measurements and settling experiments at different dosage, coagulant, polymers and more complex dissolved ions conditions.

1.7 References

Behrens, S. H., & Borkovec, M. (1999). Electrostatic interaction of colloidal surfaces with variable charge. *The Journal of Physical Chemistry B, 103*(15), 2918-2928

Buchs, B., Evangelou, M. W. H., Winkel, L. H. E., & Lenz, M. (2013). Colloidal properties of nanoparticular biogenic selenium govern environmental fate and bioremediation effectiveness. *Environmental science & technology, 47*(5), 2401-2407

Cappella, B., & Dietler, G. (1999). Force-distance curves by atomic force microscopy. *Surface science reports, 34*(1), 1-104

Chotas, H. G., Dobbins Iii, J. T., & Ravin, C. E. (1999). Principles of digital radiography with large-area, electronically readable detectors: a review of the basics. *Radiology, 210*(3), 595-599

Dowdle, P. R., & Oremland, R. S. (1998). Microbial oxidation of elemental selenium in soil slurries and bacterial cultures. *Environmental science & technology, 32*(23), 3749-3755.

Duan, J., & Gregory, J. (2003). Coagulation by hydrolysing metal salts. *Advances in colloid and interface science, 100*, 475-502

Dungan, R. S., & Frankenberger, W. T. (1999). Microbial transformations of selenium and the bioremediation of seleniferous environments. *Bioremediation Journal, 3*(3), 171-188.

Eckenfelder Jr, W. W. (2000). Industrial Water Pollution Control: Mc Graw Hill Book Company, New York.

Fitzpatrick, C. (2013). Envirogen awarded patent for fluidized bed reactor treatment of perchlorate contaminated water.

Foster, L. H., & Sumar, S. (1997). Selenium in health and disease: a review. *Critical Reviews in Food Science & Nutrition, 37*(3), 211-228

Frankenberger Jr, W. T., & Karlson, U. (1994). Microbial volatilization of selenium from soils and sediments. *Selenium in the Environment*, 369-387.

Frankenberger, W. T., & Engberg, R. A. (1998). *Environmental chemistry of selenium*: CRC Press.

Hamilton, S. J. (2004). Review of selenium toxicity in the aquatic food chain. *Science of the Total Environment, 326*(1), 1-31

Hatzinger, P. B., Greene, M. R., Frisch, S., Togna, A. P., Manning, J., & Guarini, W. J. (2000). Biological treatment of perchlorate-contaminated groundwater using fluidized bed reactors *Case studies in the remediation of chlorinated and recalcitrant compounds* (pp. 115-122): Citeseer.

Hill, C. M. (2010). Review of Available Technologies for the Removal of Selenium from Water. *Final Report, prepared for North American Metals Council (NAMC)*.

Israelachvili, J. N. (2011). *Intermolecular and surface forces: revised third edition*: Academic press.

Johnson, P. N., & Amirtharajah, A. (1983). Ferric chloride and alum as single and dual coagulants. *Journal (American Water Works Association)*, 232-239

Kapoor, A., Tanjore, S., & Viraraghavan, T. (1995). Removal of selenium from water and wastewater. *International journal of environmental studies, 49*(2), 137-147

Lemly, A. D. (2004). Aquatic selenium pollution is a global environmental safety issue. *Ecotoxicology and environmental safety, 59*(1), 44-56

Li, T., Zhu, Z., Wang, D., Yao, C., & Tang, H. (2006). Characterization of floc size, strength and structure under various coagulation mechanisms. *Powder technology, 168*(2), 104-110

Munirathinam, K., Srinivasan, R., Tudini, J. J., Sandy, T. A., & Harrison, T. D. (2011). Selenium treatment of mine water effluent in a fluidized bed reactor (FBR). *Proceedings of the Water Environment Federation, 2011*(18), 157-177

Navarro-Alarcon, M., & Cabrera-Vique, C. (2008). Selenium in food and the human body: a review. *Science of the Total Environment, 400*(1), 115-141

Oberhauser, A. F., Marszalek, P. E., Erickson, H. P., & Fernandez, J. M. (1998). The molecular elasticity of the extracellular matrix protein tenascin. *Nature, 393*(6681), 181-185

Reid, M. E., Stratton, M. S., Lillico, A. J., Fakih, M., Natarajan, R., Clark, L. C., & Marshall, J. R. (2004). A report of high-dose selenium supplementation: response and toxicities. *Journal of Trace Elements in Medicine and Biology, 18*(1), 69-74

Rief, M., Gautel, M., Oesterhelt, F., Fernandez, J. M., & Gaub, H. E. (1997). Reversible unfolding of individual titin immunoglobulin domains by AFM. *Science, 276*(5315), 1109-1112.

Rotruck, J. T., Pope, A. L., Ganther, H. E., Swanson, A. B., Hafeman, D. G., & Hoekstra, W. G. (1973). Selenium: biochemical role as a component of glutathione peroxidase. *Science, 179*(4073), 588-590.

Schott, H. (1981). Electrokinetic studies of magnesium hydroxide. *Journal of pharmaceutical sciences, 70*(5), 486-489

Semerjian, L., & Ayoub, G. M. (2003). High-pH–magnesium coagulation–flocculation in wastewater treatment. *Advances in Environmental Research, 7*(2), 389-403.

Shammas, N. K. (2005). Coagulation and flocculation *Physicochemical treatment processes* (pp. 103-139): Springer.

Smith, A. M., & Nie, S. (2009). Semiconductor nanocrystals: structure, properties, and band gap engineering. *Accounts of chemical research, 43*(2), 190-200

Sonstegard, J., Pickett, T., Harwood, J., & Johnson, D. (2008). Full scale operation of GE ABMet® biological technology for the removal of selenium from FGD wastewaters. *IWC, 8*, 31.

Staicu, L. C., Van Hullebusch, E. D., Oturan, M. A., Ackerson, C. J., & Lens, P. N. L. (2015). Removal of colloidal biogenic selenium from wastewater. *Chemosphere, 125*, 130-138

Valtiner, M., Kristiansen, K., Greene, G. W., & Israelachvili, J. N. (2011). Effect of surface roughness and electrostatic surface potentials on forces between dissimilar surfaces in aqueous solution. *Advanced materials, 23*(20), 2294-2299

Visser, J. (1972). On Hamaker constants: A comparison between Hamaker constants and Lifshitz-van der Waals constants. *Advances in colloid and interface science, 3*(4), 331-363

Wang, H., Zhang, J., & Yu, H. (2007). Elemental selenium at nano size possesses lower toxicity without compromising the fundamental effect on selenoenzymes: comparison with selenomethionine in mice. *Free Radical Biology and Medicine, 42*(10), 1524-1533

Wang, N., Hsu, C., Zhu, L., Tseng, S., & Hsu, J.-P. (2013). Influence of metal oxide nanoparticles concentration on their zeta potential. *Journal of colloid and interface science, 407*, 22-28

WHO, G. (2011). Guidelines for drinking-water quality. *World Health Organization*.

Wilber, C. G. (1980). Toxicology of selenium: a review. *Clinical toxicology, 17*(2), 171-230

Chapter 2 Experimental Techniques

2.1 Atomic force microscope (AFM)

In this project, atomic force microscope (AFM, Asylum MFP-3D) was used to measure the forces between an elemental selenium particle and different surfaces, and also to characterize the surface topography. AFM is a high-resolution scanning probe technique that is widely used to investigate the surface properties of various kinds of materials, studying topography with range of angstrom to micro level, and it is considered as one of the most advanced tools for surface force measurement (Butt, Cappella, & Kappl, 2005). AFM was invented in 1986 by IBM scientists and the first commercial AFM came shortly after in 1989.

Generally, an AFM consists of a piezo scanner, a cantilever with a probe, a laser beam source, a split photodiode and a detector-feedback electronics system as illustrated in Fig. 2.1. A cantilever with a probe (in the case of this project for force measurement is a selenium particle) at the end is attached to an actuator. The height of the cantilever is controlled by the z-piezo. When the probe approaches to the surface of sample, forces generated in-between the probe and sample lead to deflection of the cantilever governed by Hooke's law. The degree of deflection is monitored by the laser beam that is reflected to the photodiode. The photodiode transfers the signals to electronics system. Then the electronics system would generate force profiles shown on monitor. The retracting steps would be the same as approaching case.

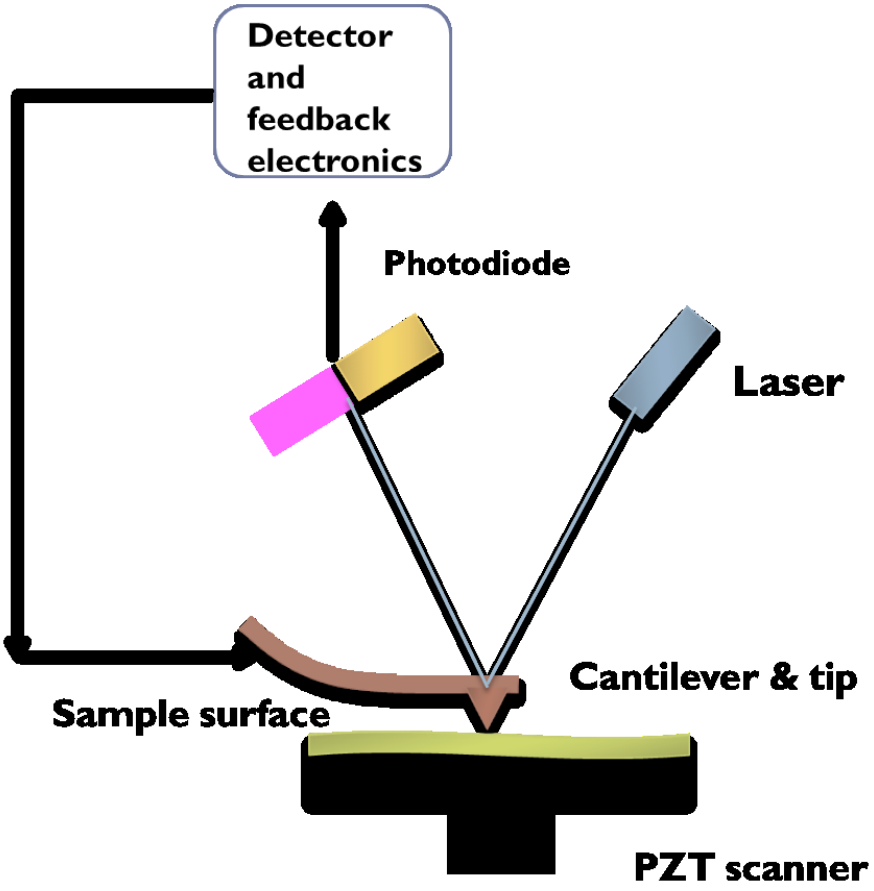

Figure 2.1. Schematic diagram of atomic force microscope. (Source: adapted from Nanotechnology – Tools and Instruments. (2011, March 2))

Moreover AFM is not the only equipment to measure the intermolecular forces between particles. Surface forces apparatus (SFA), for example, is available to directly measure the forces between two mica surface cylinders. One mica cylinder is connected to a piezoelectric translator which could controls the separation and the separation distance can be measured by using multiple beam interference fringes. The other mica cylinder is attached to a spring which the spring constant can be determined. The two cylinders have the same radius and position 90 degree to each other which the results are mathematically equivalent to the interaction between a sphere particle with the same

radius and a flat surface. Recent years, total internal reflection microscopy (TIRM) and osmotic stress method are also developed for determining the forces between lipid bilayers or macromolecules (Butt et al., 2005). Compared to the other methods, AFM is easier to operate, has less restrictions to the samples and is more commercial available with updated technologies.

2.2 Zeta potential measurement

In this project, Zetasizer Nano ZSP (Malvern Instruments Ltd) is used to measure the zeta potential of colloidal particles. Moreover, Zetasizer Nano ZSP is capable of measuring particle size and molecular weight which would suggest more information of the properties of interested materials. Generally speaking, it could measure zeta potential of particles with size range of 3 nm to 10 μm (Manual, 2003). Zeta potential would provide information of particles that is directly correlated to the tendency of flocculation (Revil, Pezard, & Glover, 1999). A schematic diagram indicating the location of zeta potential is showed in Fig. 2.2. As can be seen from the graph, positive ions closed to the negative charged particle are strong bonded to the surface. A little further away is the slipping plane and is in the region of diffusive layer where ions are loosely attached but still move with particles. The zeta potential of the particle is the potential at slipping plane.

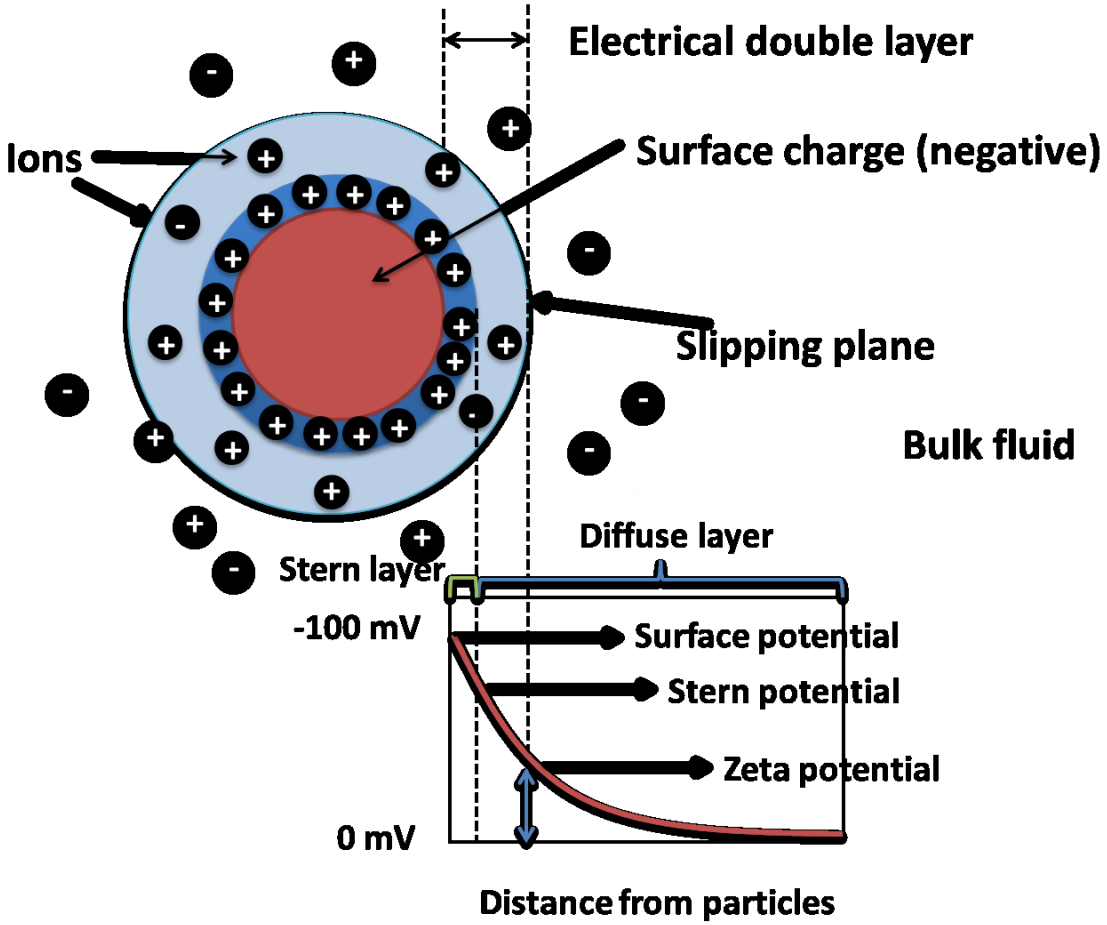

Figure 2.2. Schematic diagram representation of Zeta potential (Source: adapted from Instruments (2011))

2.3 Quartz crystal microbalance with dissipation monitoring (QCM-D)

In 1959, Sauerbrey found that there is positive correlation between resonance frequency change (Δf) of quartz crystal and mass uptake (Δm) of quartz crystal itself and proposed the Sauerbrey equation (Sauerbrey, 1959):

$$\Delta m = C\frac{\Delta f}{n} \tag{2.1}$$

where C is a constant related to the physical properties of the quartz and n is the resonance number of the sensor (n = 1, 3, 5, 7, 9, 11, 13). The resonance for the measurement always has odd number since the wave could only resonate on even harmonics. However, Sauerbrey equation is valid only when the materials adsorbed on the quartz surface is rigid and no slip happens during the process. Energy dissipation, therefore, is taking into account for the mechanical energy loss which could qualitatively investigate the structure of the adsorbed layers. The energy dissipation is defined as the ratio between energy dissipated during the oscillation and energy stored in the oscillation system:

$$\Delta D = \frac{1}{Q} = \frac{E_{Dissipated}}{2\pi E_{Stored}} \tag{2.2}$$

In 1996, Q-sense company was founded by a group of researcher at the Department of Applied Physics in Chalmers University of Technology. The model Q-sense E4 is a robust instrument that could monitor the real-time adsorption or desorption rate (i.e., Δm) and structure change (i.e., ΔD) associated with adsorbed layers. A photo of Q-sense E4 is shown in Fig. 2.3.

Figure 2.3. The photo of QCM-D setup.

A schematic of the mechanism of QCM-D experiment is shown in Fig. 2.4. As can be seen from Fig. 2.4, after an alternating current (AC) applying to the circuit, the sensor crystal starts to ocillate due to the quartz piezoelectric propertie. When a mass is adsorbed on the sensor surface, the resonance frequency would decrease. When a viscoelastic film adsored on the surface, the layer would dampen the oscillation and results in dissipation change. As can be seen in Fig. 2.4, the the viscoelastic material would have larger dissipation change.

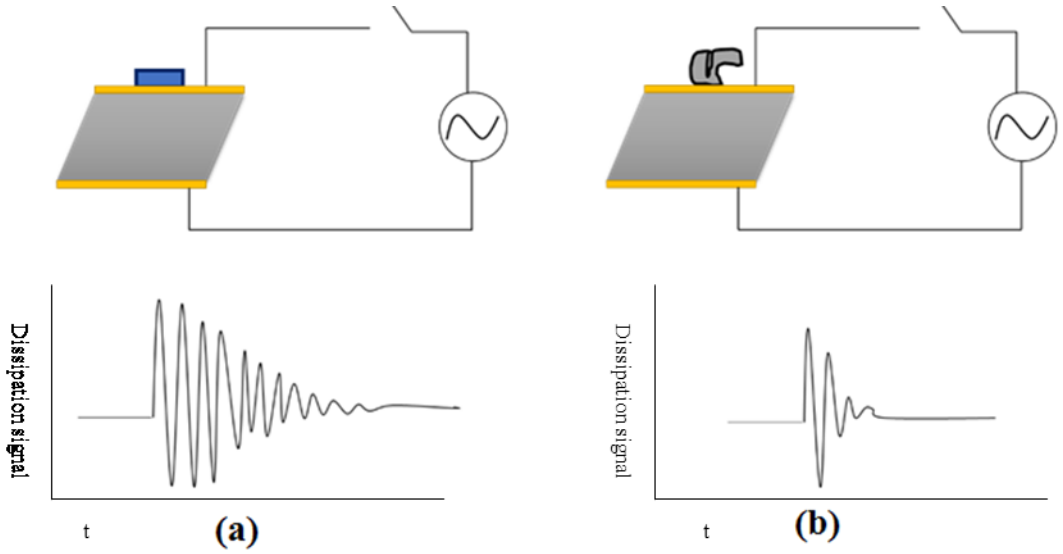

Figure 2.4. The schematic of the sensor resonance of a QCM-D experiment(a) rigid file, (b) vescoelastic film.

(Source: adapted from http://www.biolinscientific.com/technology/qcm-d-technology/)

2.4 Inductively coupled plasma mass spectrometry (ICP-MS)

The Inductively Coupled Plasma Mass Spectrometry (ICP-MS) is a very powerful mass spectrometry that can detect the concentration of elements from Li to U at the accuracy of ppb (Beauchemin D., 2008). The concentration measurement of an element is achieved by ionizing the sample with inductively coupled plasma and then using a mass spectrometer to identify and quantify these ions. Perkin Elmer Elan 6000 quadrupole ICP-MS was used in this study.

2.5 References

Beauchemin, D. (2008). Inductively coupled plasma mass spectrometry. *Analytical chemistry, 80*(12), 4455-4486

Butt, H.-J., Cappella, B., & Kappl, M. (2005). Force measurements with the atomic force microscope: Technique, interpretation and applications. *Surface science reports, 59*(1).

Instruments, M. (2011). Zeta potential: An Introduction in 30 minutes. *Zetasizer Nano Serles Technical Note. MRK654-01*.

Manual, Z. N. S. U. (2003). Malvern Instruments Ltd. *Manual Version IM, 100*, 1.23-21.26.

Nanotechnology – Tools and Instruments. (2011, March 2). Retrieved July 22, 2015, from http://www.circuitstoday.com/nanotechnology-tools-and-instruments

Revil, A., Pezard, P. A., & Glover, P. W. J. (1999). Streaming potential in porous media: 1. Theory of the zeta potential. *Journal of Geophysical Research: Solid Earth (1978–2012), 104*(B9), 20021-20031.

Sauerbrey, G. (1959). Verwendung von Schwingquarzen zur Wägung dünner Schichten und zur Mikrowägung. *Zeitschrift für physik, 155*(2), 206-222

Chapter 3 Understanding the Mechanism of Interactions between Elemental Selenium and Ferric Hydroxide in Wastewater

3.1 Introduction

After selenium (Se) was found in 1817, it has drawn lots of attention to understanding the special physical properties and important roles for biological functions (Wilber, 1980). Se is a metalloid mineral that belongs to the oxygen family in the periodic table and shares similar properties as sulfur (S) and tellurium (Te), which are well known as essential components for electronic industries such as semiconductor, photoconductor and printer drum (Chotas, Dobbins Iii, & Ravin, 1999; Smith & Nie, 2009).

Furthermore Se is a necessary nutrient element for life in trace amount, but both excess and deficient intake of Se could cause severe damage to human and animal body (Foster & Sumar, 1997; Navarro-Alarcon & Cabrera-Vique, 2008). A range of Se dietary allowance has been proposed by World Health Organization (WHO) for a suggested intake of 40 μg/day and maximum intake of 400 μg/day (WHO, 2011). In the safe intake range, it has been studied that Se plays significant roles on some proteins formation such as enzyme glutathione peroxidase (Rotruck et al., 1973). However if Se intake is insufficient, Keshanin-Beck disease, a disease of the bone, was reported to be caused by extremely low level of Se in soil in areas of northern China and eastern Siberia (Foster & Sumar, 1997). On the other hand, many cases have been investigated of mining, refinery and agriculture drainage wastewater containing high level of selenium, which could cause reproductive failures/ abnormalities in aquatic vertebrates (i.e., fish, birds and reptiles) (Frankenberger

& Engberg, 1998; Hamilton, 2004) and serious lesions of hair, skin and nails for human beings (Reid et al., 2004). Se oxyanions, selenite (SeO_3^{2-}) and selenate (SeO_4^{2-}), are the predominate forms and mostly contribute to selenium pollution in aqueous environment (Kapoor et al., 1995; Lemly, 2004), but elemental selenium (Se^0), in comparison with SeO_3^{2-} and SeO_4^{2-}, has much less toxic effect (H. Wang et al., 2007), which makes the reduction of Se oxyanions to elemental selenium a promising approach for Se removal from aqueous system.

In order to reduce Se oxyanions to elemental selenium, biological reduction technologies have been studied comprehensively and proved to be industrially feasible (Hill, 2010; Munirathinam et al., 2011). Especially fluidized bed reactor (FBR) and ABMet® technologies both have been conducted on pilot and full scale for treating mining and coal fire power plant wastewater (Fitzpatrick, 2013; Hatzinger et al., 2000; Sonstegard et al., 2008). There are a number of microorganisms capable for Se oxyanion reduction to form insoluble elemental selenium nanoparticles (SeNPs) by bacteria respiration process under either aerobic or anaerobic aqueous environments (Dungan & Frankenberger, 1999; Frankenberger Jr & Karlson, 1994). After reduction process, the product biogenerated elemental selenium shows stable colloidal properties in solution since SeNPs have size of 50 to 500 nm and are highly negatively charged (i.e., around - 40 mV) at natural pH (i.e., pH 6 – 8).Therefore particle removal by gravity settling could not be applied (Buchs et al., 2013). Coagulation and flocculation processes using trivalent metal salts are found to be very effective to remove colloidal particle impurities (Duan & Gregory, 2003). Recent results have shown that metal salts, ferric chloride ($FeCl_3$) and aluminum sulfate

($Al_2(SO4)_3$), are effective coagulants for removing biogenerated SeNPs with 42% and 92% turbidity removal respectively (Staicu, Van Hullebusch, Oturan, Ackerson, & Lens, 2015).

Trivalent metal salts in coagulation and flocculation processes mainly contribute two effects on removing impurities: charge neutralization and sweep flocculation (Duan & Gregory, 2003; Li, Zhu, Wang, Yao, & Tang, 2006). For charge neutralization process, trivalent metal salts can produce strongly cationic hydroxide complexes that could adsorb SeNPs and neutralize the surface charges of SeNPs. As more metal salts were added into wastewater, sweep flocculation is promoted and the insoluble precipitates are formed, which allow colloidal particles to be enmeshed into the insoluble amorphous coagulants and removed by settling.

Although researchers have intensively studied the mechanisms of ferric hydroxide ($Fe(OH)_3$) coagulation and flocculation processes, a deeper understanding of $Fe(OH)_3$ interacting with impurities at interface is still remained to be further investigated. For the case of SeNPs removal, interactions between SeNPs and $Fe(OH)_3$ is still not clear, and no direct force measurement has been done yet, which is of both fundamentally and practically importance.

In this study, precipitation and settling of SeNPs in a coal mining wastewater were investigated with $Fe(OH)_3$ prepared from $FeCl_3$ as coagulant. The effects of conditions (i.e., pH value) on the settling efficiency were performed. To better understand the interaction mechanism between SeNPs and $Fe(OH)_3$, Atomic Force Microscopy (AFM) was applied to directly measure the forces between the two surfaces, and Quartz Crystal Microbalance with Dissipation (QCM-D) measurement was also conducted.

3.2 Materials and Methods

3.2.1 Materials

Elemental selenium particles in aqueous solution were supplied by MK Impex Corporation (the average particle size is 100 nm and solution concentration is 0.1 mg/mL). Iron (III) chloride anhydrous, $FeCl_3$ (98% pure) was supplied by Acros Organics. Epoxy adhesive (EP41S-1HT) were purchased from Master Bond. Hydrochloric acid, HCl (1 N) and sodium hydroxide, NaOH (1 N) were supplied by Fisher Scientific Company. Milli-Q water was used in preparing stock $FeCl_3$ solution and lavation process. The wastewater was provided from the effluent of secondary biological fluidized bed reactor (FBR). Selenium oxyanions in wastewater were reduced to elemental selenium after biological process. Besides selenium, the content of wastewater has high concentration of calcium and magnesium ions.

3.2.2 Settling Test

Settling tests were conducted in this study to determine the proper pH values for SeNPs settling. Each beaker contained 100 mL wastewater. Freshly prepared $FeCl_3$ solution (50 ppm, 1 ppm = 1 mg/L) was first added into the sample wastewater with mixing at 100 rpm for 1 min, followed by a slow mixing at 30 rpm for 10 min. The pH effect on removal efficiency was performed by adjusting pH of each sample with 1 N HCl and NaOH. After each test, the supernatant was collected for further Inductively Coupled Plasma – Mass Spectrometry (ICP-MS) analysis for determining selenium concentration.

3.2.3 Biological FBR wastewater and interactions of elemental selenium and $Fe(OH)_3$ analysis.

A Perkin Elmers's Elan 6000 ICP-MS was used to test the selenium element concentration. Zeta potential measurement was performed by using Zetasizer Nano ZSP with disposable folded capillary cells supported by Malvern Instrument Ltd. QCM-D, Q-Sense E4, was used to study the adsorption behavior of elemental selenium on $Fe(OH)_3$ sensor.

3.2.4 AFM experiments and theoretical calculation

All AFM experiments were conducted on MFP-3D AFM (Asylum Research). Rectangular silicon AFM probes with spring constant of 42 N/m and triangular tipless silicon nitride AFM cantilevers with spring constant of 0.06-0.35 N/m were purchased from Bruker. Selenium particle suspension was dropped on a glass slide and dried in air. Epoxy adhesive was placed on a glass slide and a trace amount of epoxy adhesive was picked up by lowering down a tipless AFM cantilever. Then a selenium particle was picked up by the tipless AFM cantilever with epoxy adhesive, and the resulting assembly was dried in air for at least 24 h. The Se probe was rinsed with ethanol and Milli-Q water before each use. The force-distance curves were obtained in aqueous solutions by approaching and retracting a selenium sphere probe on a substrate. The approaching and retracting velocity is 1.98 $\mu m\ s^{-1}$.

Fig. 3.1 shows the optical microscopic image of an elemental selenium sphere particle that is glued to the end of the cantilever and to be used for force measurement. The diameter of the selenium sphere is 3.7 μm.

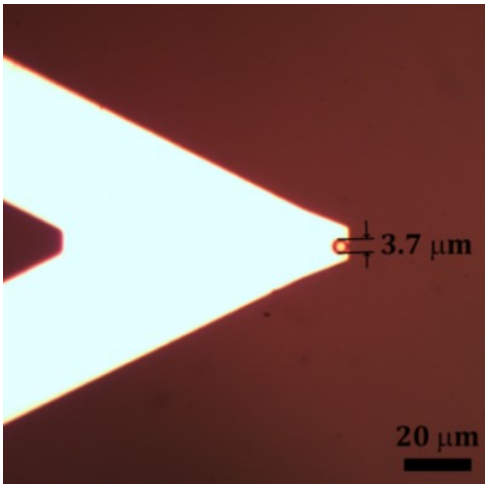

Figure 3.1. Microscopic image of elemental selenium sphere particle attached on a tipless cantilever

The Derjaguin-Landau-Verwey-Overbeek (DLVO) forces (F_{dlvo}) model, which includes Van der Waals forces (F_{vdw}) and electric double layer forces (F_{edl}) was used to describe the surface forces existing between Se probe and $Fe(OH)_3$ surface. A constant charge DLVO model was applied for theoretical calculation in the case of a sphere approaching to an infinite flat substrate (Cappella & Dietler, 1999; J. N. Israelachvili, 2011). The equations are described as follows:

$$F_{\mathrm{vdw}} = -\frac{A_{Se-water-Fe(OH)_3} R}{6D^2} \tag{3.1}$$

$$F_{\mathrm{edl}} = \frac{\pi}{\varepsilon\varepsilon_0 {\kappa_D}^2}[({\sigma_T}^2 + {\sigma_s}^2)(\mathrm{e}^{-2\kappa_D R} + 2K_D R - 1)\mathrm{e}^{-2\kappa_D D} + 4\sigma_T\sigma_s(\mathrm{e}^{-\kappa_D R} + \kappa_D R - 1)\mathrm{e}^{-\kappa_D R}] \tag{3.2}$$

Where A is the Hamaker constant between Se and $Fe(OH)_3$ in bulk water media, R is the Se probe radius, D is the separation distance between Se probe and flat $Fe(OH)_3$ surface, ε is the relative permittivity, ε_0 is the vacuum permittivity, σ_T is the tip surface charge

density, σ_s is the substrate surface charge density and κ is the Debye length. The Hamaker constant is approximated by Equation 3.3 (J. N. Israelachvili, 2011):

$$A_{Se-water-Fe(OH)_3} \approx \sqrt{A_{Fe(OH)_3-water-Fe(OH)_3} \times A_{Se-water-Se}} \quad (3.3)$$

Where $A_{Fe(OH)_3-water-Fe(OH)_3}$ and $A_{Se-water-Se}$ are Hamaker constants for interactions between same materials in aqueous medium. Those Hamaker constant values are obtained from literatures (Behrens & Borkovec, 1999; Visser, 1972).

The charge density is approximated by Equation 3.4 (J. N. Israelachvili, 2011):

$$\sigma = \sqrt{8\varepsilon_0 \varepsilon kT[\mathrm{NaCl}]}\sinh(\frac{e\psi_0}{2kT}) \quad (3.4)$$

Where T is the temperature, [NaCl] is the salt concentration and ψ_0 is the surface potential.

3.3 Results and discussion

3.3.1 Wastewater characterization

Table 3.1 summarizes the major characteristics of the FBR wastewater. It showed natural pH with very low turbidity; however, there were great amount of dissolved salt impurities. The elemental selenium to be treated were around 690 ppb. The high content of Ca^{2+} and Mg^{2+} dissolved ions were found to affect the performance of water treatment results, which will be discussed later.

Table 3.1. Properties of the biological treated wastewater

Parameters	Units	Value
pH	-	8.0
Turbidity	-	0.981
Ca^{2+} and Mg^{2+}	mg/L	904.0
Salinity (Na^{+}, Ca^{2+} and Mg^{2+})	mg/L	919.4
Se^{0}	mg/L	0.69

Fig. 3.2 shows the zeta potential variation of wastewater as a function of pH. As can be seen from the curve, zeta potential values remained changes slightly as a function of pH. Most of the values were in between - 5 mV and - 10 mV. At pH 10 and 11, white participates occurred, because calcium and magnesium ions were precipitated out due to high concentration of hydroxide ions (Semerjian & Ayoub, 2003). Furthermore zeta potential at pH 11 dropped to -16.0 ± 0.99 mV when the large amount of negative calcium and magnesium precipitates was formed in the solution (Schott, 1981). And the zeta potential values were still in the range of -5 mV to -10 mV (red dots) after taking the supernatant of the solution for the measurement of zeta potential at pH 10 and 11. Since the ionic strength of wastewater is high, the electric double layer was compressed; therefore, the zeta potential showed a narrow range of variation as a function of pH.

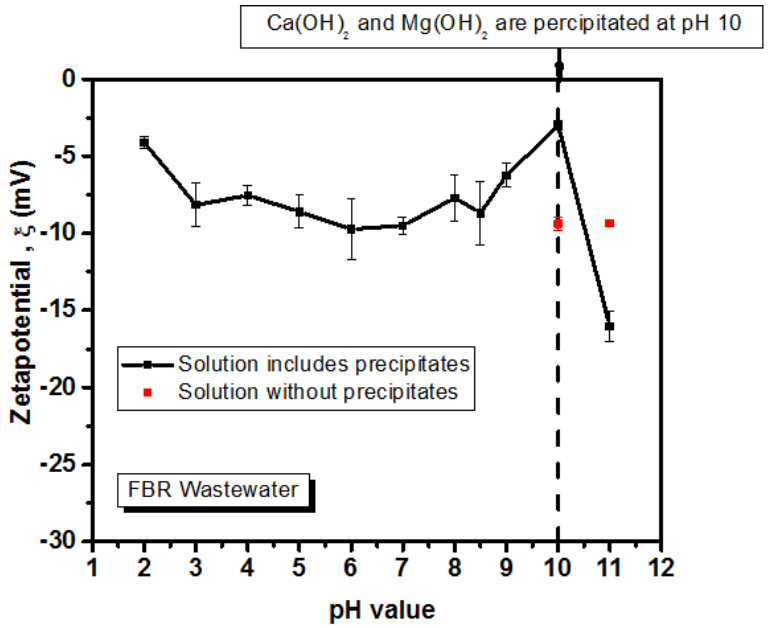

Figure 3.2. Zeta potential of FBR wastewater as a function of pH. Note that after pH 10, precipitates occurred in the solution.

3.3.2 Effect of $FeCl_3$ on SeNPs removal in wastewater

Fig. 3.3 shows the settling test on SeNPs removal from FBR wastewater. With addition of 50 ppm $FeCl_3$, the removal efficiency first decreased from pH 6 to 7 (from 72.4 ± 2.76 % to 37.0 ± 6.30 %), then it increased to 68.3 ± 3.17 % at pH 8, and dropped to 40.8±5.91 % at pH 9. This "W" shaped curve can be contributed to three combined effects: surface charges of $Fe(OH)_3$ and SeNPs, solubility of Fe species, Ca^{2+} and Mg^{2+} ions precipitations.

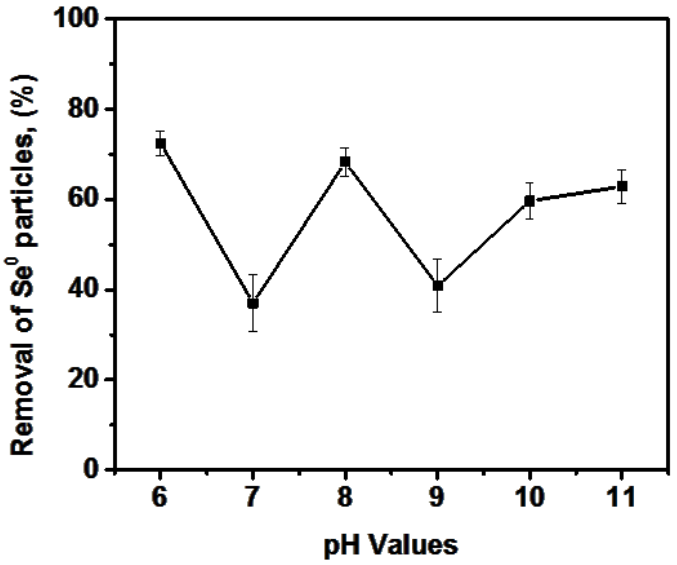

Figure 3.3. Elemental selenium removal efficiency as a function of pH at 50 ppm $FeCl_3$.

3.3.3 Zeta potentials of elemental selenium particles and the precipitates of iron salt

Fig. 3.4a shows the zeta potentials of SeNPs by as a function of pH. With increase of pH, the surface charge was being from positive to negative. The highest value point was 24.7±1.57 mV at pH 2.5 and the lowest value was -33.2±1.81 mV at pH 6 followed by a negative zeta potential plateau. The point of zero charge (PZC) is at pH 3.87 (extrapolated). Meanwhile, two sharp drop regions can be seen from 14.2± 1.23 mV to -5.1±1.58 mV and from -14.4±1.18 mV to -33.2±1.81 mV corresponding to pH from 3.5 to 4 and from 5.5 to 6 respectively.

Fig. 3.4b shows zeta potentials transition of 1 and 50 ppm of $Fe(OH)_3$ in 1 mM NaCl solution. In general, zeta potentials of $Fe(OH)_3$ shifted negatively with decrease of dosage

which supported by the similar results from Wang, Nan, et al.(N. Wang, Hsu, Zhu, Tseng, & Hsu, 2013).

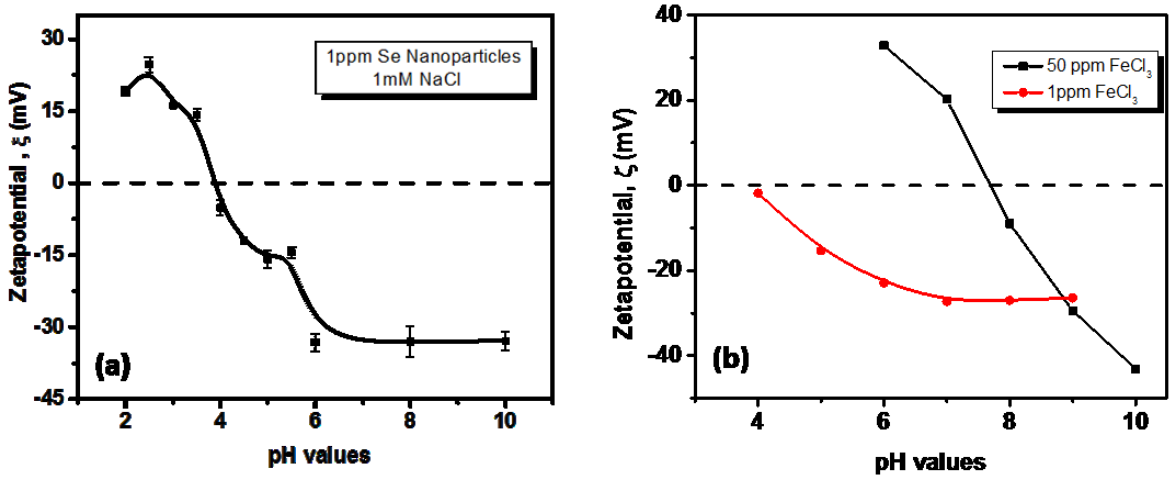

Figure 3.4. (a) Elemental selenium zeta potential change as a function of pH in 1mM NaCl solution, (b) zeta potential of $FeCl_3$ precipitates as a function of pH in 1 mM NaCl solution.

As can be seen from Fig. 3.4a, SeNPs were highly negative charges with pH higher than 6. On the other hand 50 ppm amorphous $Fe(OH)_3$ had point of zero charge (PZC) at pH 7.69 (extrapolated) as shown in Fig. 3.4b, and zeta potential of $Fe(OH)_3$ dropped from around 30 mV to -40 mV from pH 6 to 10. Attraction between SeNPs and $Fe(OH)_3$ decreased; therefore, removal efficiency decreased from pH 6 to 7, which suggested that the removal mechanism at low pH was described as adsorption-destabilization process (Duan & Gregory, 2003; Johnson & Amirtharajah, 1983). At higher pH, interactions between SeNPs and $Fe(OH)_3$ migrated from attraction to repulsion, however, sweep flocculation plays more important roles on elemental selenium removal. According to Jinming, and John Gregory. 2003, insoluble $Fe(OH)_3$ had highest mole fraction at pH 8,

and more SeNPs were enmeshed into the amorphous $Fe(OH)_3$, which removal efficiency increased from pH 7 to 8. After pH 8, the drop of removal efficiency can be explained by that the concentration of insoluble $Fe(OH)_3$ decreased and electric double layer repulsion became significant between $Fe(OH)_3$ and elemental selenium. At pH 10 and 11, Ca^{2+} and Mg^{2+} precipitates ($Ca(OH)_2$ and $Mg(OH)_2$) settled out of waste water solution. The precipitate had large surface area and positive surface charges, which helped elemental selenium adsorption and removal, therefore; the removal efficiency increased from pH 10 to 11 (Semerjian & Ayoub, 2003).

3.3.4 Interactions of $Fe(OH)_3$ and elemental selenium particles

Fig. 3.5 shows the frequency and dissipation changes of the $Fe(OH)_3$ sensor induced adding 1 ppm SeNPs adsorption in 1 mM NaCl solution. After injection of SeNPs for 3500 s, the frequency decreased from 0 Hz to around -15 Hz, and dissipation increased from 0 to around 2.2×10^{-6}. Rinsing with NaCl solution started at 4000 s to remove all the particles that were not well adsorbed on the sensor surface. The negative frequency shift indicated that the mass increased on the sensor which is due to SeNPs adsorption on the surface. The increase of dissipation change could be attributed to that SeNPs film formed on the sensor surface.

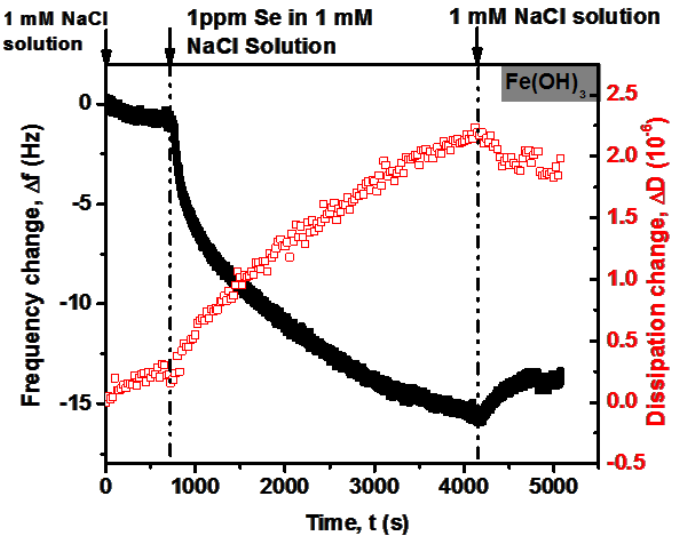

Figure 3.5. QCM-D experiment of 1 ppm SeNPs adsorption on $Fe(OH)_3$ sensor in 1 mM NaCl solution.

3.3.5. AFM forces measurement

Fig. 3.6 shows the AFM topographic images of $Fe(OH)_3$ sensor in air, in 1mM NaCl solution and in 0.1 M NaCl solution. As illustrated in Fig. 3.6a, $Fe(OH)_3$ sensor surface in air shows low roughness (R_q) of 1.043nm. When the image was taken in 1 mM NaCl solution, a substantial changes in morphology was observed as shown in Fig. 3.6b. The granular bright dots corresponded to higher elevation of insoluble $Fe(OH)_3$ molecules than the surroundings. This could be explained by the polymerization behavior of $Fe(OH)_3$ (i.e., $Fe_2(OH)_2^{4+}$) in water solution (Eckenfelder Jr, 2000; Shammas, 2005), and the polymer-like $Fe(OH)_3$ were stretched out of sensor surface. As results, R_q of $Fe(OH)_3$ surface increased to 4.634 nm. In contrast, the density of granular bright dots decreased when the surface was immersed in 0.1 M NaCl solution as shown in Fig. 3.6c. Higher salt concentration, in this case, compressed the electric double layer of $Fe(OH)_3$ and the

polymer-like $Fe(OH)_3$ were flattened on surface. The R_q of $Fe(OH)_3$ surface dropped to 3.974 nm in 0.1 M NaCl solution.

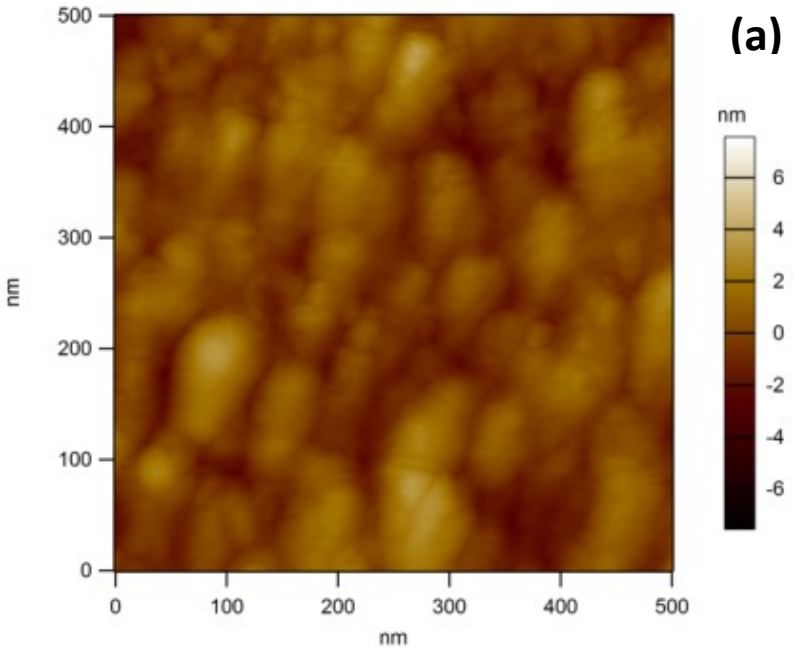

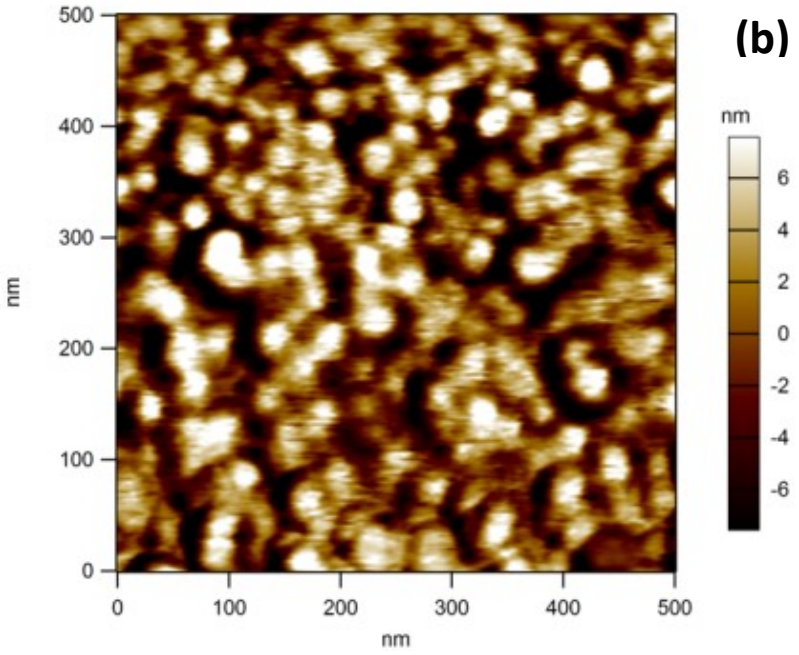

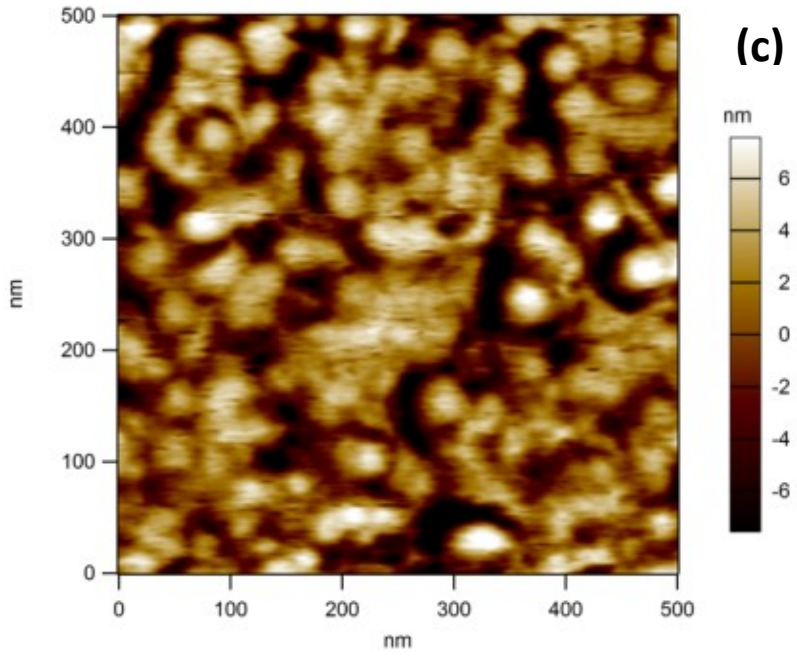

Figure 3.6. AFM topographic images of $Fe(OH)_3$ sensor in (a) air, (b) in 1 mM NaCl solution, (c) in 0.1 M NaCl solution. Images are 500 nm × 500 nm.

Fig. 3.7 and 3.8 shows the interactions forces between elemental selenium sphere and $Fe(OH)_3$. At high salt concentration, there are no long-range repulsive forces existing since the electric double layer is compressed. Van der Waals forces would dominate the system, but the theoretical prediction did not predict the forces curves very well, because the high surface roughness (around 4 nm) of $Fe(OH)_3$ prevented measurements of Van der Waals forces at short distance (J. N. Israelachvili, 2011). At low salt concentration, long-range electric double layer forces can be observed from Fig. 3.8. The double layer repulsive forces increased with increase of pH from 5 to 9. AFM force measurement used $Fe(OH)_3$ coated senor substrate that can be treated as low concentration $Fe(OH)_3$ dissolved in bulk solution, and zeta potential of low dosage of $Fe(OH)_3$ (i.e., 1ppm $FeCl_3$ in Fig. 3.4b) could better represent the surface charge of the substrate. The theoretically fitted surface potential of $Fe(OH)_3$ in 1 mM NaCl are -43 mV, -43 mV and -46 mV for pH 5.0, 7.5 and 9.0

respectively, which were much more negative than the values obtained from 1 ppm $FeCl_3$ zeta potential measurement shown in Fig. 3.4b. According to Valtiner, Kristiansen, Greene, and Israelachvili (2011), the rough surfaces had larger surface area for anion (i.e., Cl^- ions) adsorption than smooth surfaces, which enhanced the electric double layer forces; therefore, the theoretically fitted potential values were lower than measured zeta potentials.

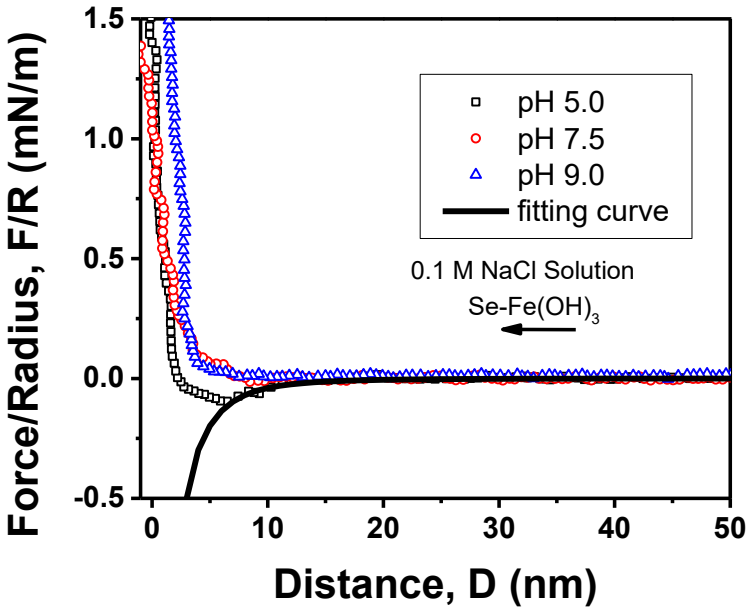

Figure 3.7. AFM force measurement between Se probe and $Fe(OH)_3$ surface. Approaching curve in 0.1 M NaCl solution.

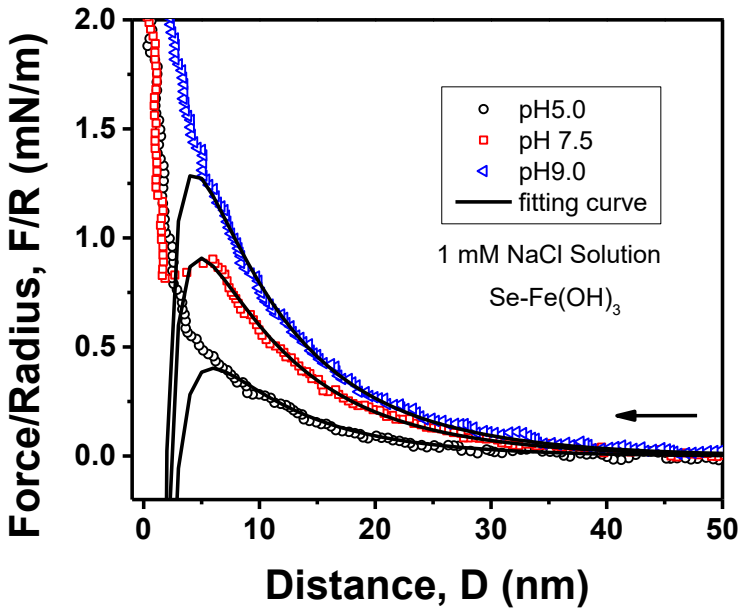

Figure 3.8. AFM force measurement between Se probe and $Fe(OH)_3$ surface. Approaching curve in 1 mM NaCl solution at pH 5.0, 7.5 and 9.0. The solid lines are the theoretical calculation with $A = 5.91 \times 10^{-20}$ J; tip potential ψ_T=-15 mV, substrate potential ψ_S=-43 mV, at pH 5; ψ_T=-32 mV, ψ_S=-43 mV, at pH 7.5; ψ_T=-35 mV, ψ_S=-46 mV, at pH 9.

From Fig. 3.9, both retract curves show worm-like chain behavior which are corresponding to the $Fe(OH)_3$ polymer behavior in solution. Similar patterns had been found from other polymer force measurements (Oberhauser, Marszalek, Erickson, & Fernandez, 1998; Rief, Gautel, Oesterhelt, Fernandez, & Gaub, 1997). Moreover, the adhesion force roughly decreases with the increasing pH since the electric double layer repulsion forces increased with increasing pH. Comparing Fig. 3.9a to 3.9b, adhesion force in 1 mM NaCl had longer range since $Fe(OH)_3$ stretched more at low salt concentration, which was proved by the AFM images shown in Fig. 3.6.

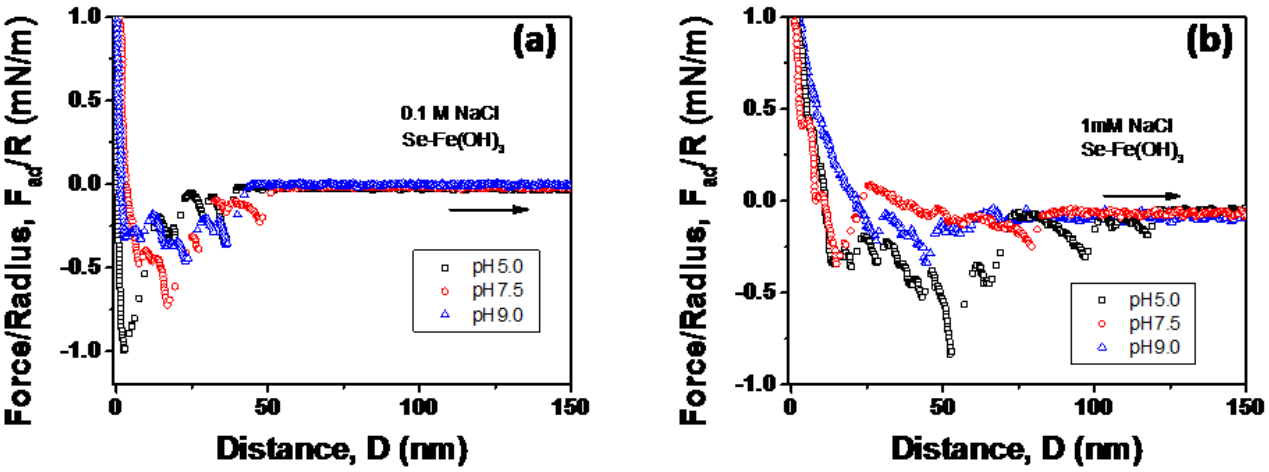

Figure 3.9. AFM force measurement between Se probe and $Fe(OH)_3$ surface. (a) Retract curve in 0.1 M NaCl solution, (b) Retract curve in 1mM NaCl solution.

An illustration of the impact from NaCl concentration was shown in Fig. 3.10. As there were high saline content in FBR wastewater, the force curve and morphology of $Fe(OH)_3$ in 0.1 M NaCl tended to represent the mechanism of elemental selenium removal. The electric double layer forces showed less impact on elemental selenium removal. Moreover more polymer behaved $Fe(OH)_3$ would be expected to prevent the detachment of SeNPs in real situation since amorphous $Fe(OH)_3$ has more available surface areas compared to $Fe(OH)_3$ coated substrate which only one side was used in AFM and QCM-D measurement.

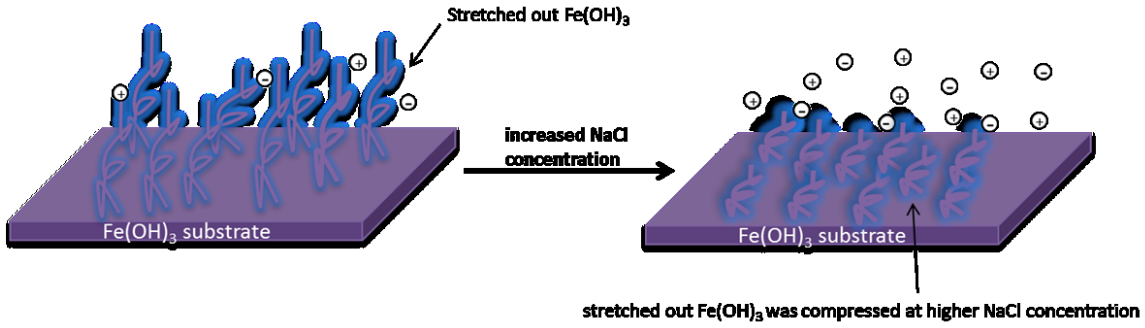

Figure 3.10. Schematic diagram of the impact of NaCl concentration on the conformation of $Fe(OH)_3$ surfaces (a) in 1 mM NaCl solution, (b) in 0.1 M NaCl solution.

3.4. Conclusions

The mechanism of interactions between SeNPs and $Fe(OH)_3$ were investigated in this study by understanding the morphology of $Fe(OH)_3$, surface charges of SeNPs and $Fe(OH)_3$ and forces acting between Se particles and $Fe(OH)_3$. When $FeCl_3$ were injected into FBR wastewater, the amorphous $Fe(OH)_3$ were formed form $FeCl_3$ hydrolysis. The Se^0 nano particles were absorbed on amorphous $Fe(OH)_3$ governed by Van der Waals force as the electric double layers were compressed in high salt solution. $Fe(OH)_3$ had polymer-like behavior at the boundary of the surface and depressed by higher salt concentration. For the best $Fe(OH)_3$ performance, the settling condition were suggested to be around pH 8, since the amorphous $Fe(OH)_3$ had the most in content and more polymer behaved $Fe(OH)_3$ could 'trap' SeNPs, which enhanced the sweep flocculation behavior. Our results first time showed some insights and explanations on the mechanism of amorphous $Fe(OH)_3$ coagulant on selenium nano particles removal at nano level.

3.5. References

Behrens, S. H., & Borkovec, M. (1999). Electrostatic interaction of colloidal surfaces with variable charge. *The Journal of Physical Chemistry B, 103*(15), 2918-2928

Buchs, B., Evangelou, M. W. H., Winkel, L. H. E., & Lenz, M. (2013). Colloidal properties of nanoparticular biogenic selenium govern environmental fate and bioremediation effectiveness. *Environmental science & technology, 47*(5), 2401-2407

Cappella, B., & Dietler, G. (1999). Force-distance curves by atomic force microscopy. *Surface science reports, 34*(1), 1-104

Chotas, H. G., Dobbins Iii, J. T., & Ravin, C. E. (1999). Principles of digital radiography with large-area, electronically readable detectors: a review of the basics. *Radiology, 210*(3), 595-599

Duan, J., & Gregory, J. (2003). Coagulation by hydrolysing metal salts. *Advances in colloid and interface science, 100*, 475-502

Dungan, R. S., & Frankenberger, W. T. (1999). Microbial transformations of selenium and the bioremediation of seleniferous environments. *Bioremediation Journal, 3*(3), 171-188.

Eckenfelder Jr, W. W. (2000). Industrial Water Pollution Control: Mc Graw Hill Book Company, New York.

Fitzpatrick, C. (2013). Envirogen awarded patent for fluidized bed reactor treatment of perchlorate contaminated water.

Foster, L. H., & Sumar, S. (1997). Selenium in health and disease: a review. *Critical Reviews in Food Science & Nutrition, 37*(3), 211-228

Frankenberger Jr, W. T., & Karlson, U. (1994). Microbial volatilization of selenium from soils and sediments. *Selenium in the Environment*, 369-387.

Frankenberger, W. T., & Engberg, R. A. (1998). *Environmental chemistry of selenium*: CRC Press.

Hamilton, S. J. (2004). Review of selenium toxicity in the aquatic food chain. *Science of the Total Environment, 326*(1), 1-31

Hatzinger, P. B., Greene, M. R., Frisch, S., Togna, A. P., Manning, J., & Guarini, W. J. (2000). Biological treatment of perchlorate-contaminated groundwater using fluidized bed reactors *Case studies in the remediation of chlorinated and recalcitrant compounds* (pp. 115-122): Citeseer.

Hill, C. M. (2010). Review of Available Technologies for the Removal of Selenium from Water. *Final Report, prepared for North American Metals Council (NAMC)*.

Israelachvili, J. N. (2011). *Intermolecular and surface forces: revised third edition*: Academic press.

Johnson, P. N., & Amirtharajah, A. (1983). Ferric chloride and alum as single and dual coagulants. *Journal (American Water Works Association)*, 232-239

Kapoor, A., Tanjore, S., & Viraraghavan, T. (1995). Removal of selenium from water and wastewater. *International journal of environmental studies, 49*(2), 137-147

Lemly, A. D. (2004). Aquatic selenium pollution is a global environmental safety issue. *Ecotoxicology and environmental safety, 59*(1), 44-56

Li, T., Zhu, Z., Wang, D., Yao, C., & Tang, H. (2006). Characterization of floc size, strength and structure under various coagulation mechanisms. *Powder technology, 168*(2), 104-110

Munirathinam, K., Srinivasan, R., Tudini, J. J., Sandy, T. A., & Harrison, T. D. (2011). Selenium treatment of mine water effluent in a fluidized bed reactor (FBR). *Proceedings of the Water Environment Federation, 2011*(18), 157-177

Navarro-Alarcon, M., & Cabrera-Vique, C. (2008). Selenium in food and the human body: a review. *Science of the Total Environment, 400*(1), 115-141

Oberhauser, A. F., Marszalek, P. E., Erickson, H. P., & Fernandez, J. M. (1998). The molecular elasticity of the extracellular matrix protein tenascin. *Nature, 393*(6681), 181-185

Reid, M. E., Stratton, M. S., Lillico, A. J., Fakih, M., Natarajan, R., Clark, L. C., & Marshall, J. R. (2004). A report of high-dose selenium supplementation: response and toxicities. *Journal of Trace Elements in Medicine and Biology, 18*(1), 69-74

Rief, M., Gautel, M., Oesterhelt, F., Fernandez, J. M., & Gaub, H. E. (1997). Reversible unfolding of individual titin immunoglobulin domains by AFM. *Science, 276*(5315), 1109-1112.

Rotruck, J. T., Pope, A. L., Ganther, H. E., Swanson, A. B., Hafeman, D. G., & Hoekstra, W. G. (1973). Selenium: biochemical role as a component of glutathione peroxidase. *Science, 179*(4073), 588-590.

Schott, H. (1981). Electrokinetic studies of magnesium hydroxide. *Journal of pharmaceutical sciences, 70*(5), 486-489

Semerjian, L., & Ayoub, G. M. (2003). High-pH–magnesium coagulation–flocculation in wastewater treatment. *Advances in Environmental Research, 7*(2), 389-403.

Shammas, N. K. (2005). Coagulation and flocculation *Physicochemical treatment processes* (pp. 103-139): Springer.

Smith, A. M., & Nie, S. (2009). Semiconductor nanocrystals: structure, properties, and band gap engineering. *Accounts of chemical research, 43*(2), 190-200

Sonstegard, J., Pickett, T., Harwood, J., & Johnson, D. (2008). Full scale operation of GE ABMet® biological technology for the removal of selenium from FGD wastewaters. *IWC, 8*, 31.

Staicu, L. C., Van Hullebusch, E. D., Oturan, M. A., Ackerson, C. J., & Lens, P. N. L. (2015). Removal of colloidal biogenic selenium from wastewater. *Chemosphere, 125*, 130-138

Valtiner, M., Kristiansen, K., Greene, G. W., & Israelachvili, J. N. (2011). Effect of surface roughness and electrostatic surface potentials on forces between dissimilar surfaces in aqueous solution. *Advanced materials, 23*(20), 2294-2299

Visser, J. (1972). On Hamaker constants: A comparison between Hamaker constants and Lifshitz-van der Waals constants. *Advances in colloid and interface science, 3*(4), 331-363

Wang, H., Zhang, J., & Yu, H. (2007). Elemental selenium at nano size possesses lower toxicity without compromising the fundamental effect on selenoenzymes: comparison with selenomethionine in mice. *Free Radical Biology and Medicine, 42*(10), 1524-1533

Wang, N., Hsu, C., Zhu, L., Tseng, S., & Hsu, J.-P. (2013). Influence of metal oxide nanoparticles concentration on their zeta potential. *Journal of colloid and interface science, 407*, 22-28

WHO, G. (2011). Guidelines for drinking-water quality. *World Health Organization*.

Wilber, C. G. (1980). Toxicology of selenium: a review. *Clinical toxicology, 17*(2), 171-230

Chapter 4 Investigation of Interaction between Elemental Selenium and Hydrophilic/Hydrophobic Surface: Direct Force Measurement Using AFM

4.1 Introduction

Selenium (Se) is a metalloid element that is chemically similar to sulfur and tellurium (Oremland et al., 2004). In natural environment, selenium exists with chemical forms of: selenide (Se^{2-}), amorphous or polymeric elemental selenium (Se^{0}), selenite (SeO_3^{2-}), selenate (SeO_4^{2-}) and organic selenium. The essential trace selenium plays a fundamental role in human health. It is a component of several major metabolic pathways including thyroid hormone metabolism, antioxidant defense systems, and immune function (Rayman, 2000). Selenium has unusual photo-optical and semiconducting physical properties and has industrial applications in devices such as photocopiers, microelectronic circuits, photovoltaic cells, rectifiers, photographic exposure meters, xerography, and antibacterial (Ma, Qi, Shen, & Ma, 2005; Oremland et al., 2004; Q. Wang & Webster, 2012).

In humans, selenium has one of the narrowest ranges between dietary deficiency (<40 μg per day) and toxic levels (> 400 μg per day). Concerning if the adverse effects resulting from exposure to excessive levels of selenium, a guideline value of less than 0.04 mg/L (40 μg/L or 40 ppb) selenium in drinking-water is given by the World Health Organization (WHO) (WHO, 2011). Excessive selenium can be normally accumulated through mine drainage water, industrial wastewater and agricultural drainage water, and may dramatically affect the aquatic organism and the quality of the water received by

downstream communities. Selenium has a complete biogeochemical cycle in nature, with microbial redox reactions leading both to and from all of its oxidation states (Dowdle & Oremland, 1998; Herbel, Blum, Oremland, & Borglin, 2003). However, the selenium species present in water are mainly oxyanions (SeO_4^{2-} and SeO_3^{2-}), which are more mobile and toxic than the other forms of selenium. An important component of this cycle is the reduction of SeO_4^{2-} and SeO_3^{2-} to Se^0 in reactions that could be catalyzed by microorganisms, which has been applied for selenium water treatment (Kashiwa, Nishimoto, Takahashi, Ike, & Fujita, 2000; Kuroda et al., 2011; Soda et al., 2011; Steinberg & Oremland, 1990; Zhang & Frankenberger, 2005). In the process of bioreduction, there may be intracellular and/or extracellular elemental selenium production, and the intracellular elemental selenium may be transported out of bacterial cells through membrane with the help of a membrane reductase or in a membrane vesicular (Kessi, Ramuz, Wehrli, Spycher, & Bachofen, 1999; Lampis et al., 2014; Losi & Frankenberger, 1997), in which the intermolecular and surface interactions of elemental selenium and membrane are involved. The extracellular elemental selenium are particles normally well dispersed in aqueous solutions due to their strong electrical charge, and are required for proper settling disposal to avoid secondary contamination of environment (Buchs et al., 2013; Staicu, van Hullebusch, Lens, Pilon-Smits, & Oturan, 2014; Zhang, Zahir, & Frankenberger, 2004). The efficiency of elemental selenium settling is governed by the surface interactions between elemental selenium particles and other species in the colloid system. The collected elemental selenium particles may have biomedical applications (Chaudhary, Umar, & Mehta, 2014) or be used on devices (Narayanan & Sakthivel, 2010). Therefore, the surface interactions between elemental selenium and other solid species are

involved in biological system, water treatment, and device applications.

Since 1989, the atomic force microscope (AFM) has emerged as a useful tool for studying surface interactions by means of force-distance curves (Cappella & Dietler, 1999). The key element of the AFM is a cantilever with a probe having a radius of curvature on the order of nanometers. When the probe is brought into proximity of a sample surface, forces between the probe and the sample lead to a deflection of the cantilever according to Hooke's law. The force-distance curve measurement was then further conducted in liquids (Weisenhorn, Hansma, Albrecht, & Quate, 1989) by modifying AFM probes (Frisbie, Rozsnyai, Noy, Wrighton, & Lieber, 1994) and by fabricating various colloidal probes (Butt, 1991; Dagastine, Stevens, Chan, & Grieser, 2004; Ducker, Senden, & Pashley, 1991; Vakarelski et al., 2008). The tenability of materials of AFM probe and substrate facilitated many studies on different interactions between various surfaces in several liquid environments using AFM. In 1991, Ducker et al. (1991) attached a silica sphere of 3.5 μm in radius onto AFM cantilever and measured colloidal forces by approaching the silica sphere towards a silicon wafer. The results obtained were found to be consistent with DLVO (Derjaguin-Landau-Verwey-Overbeek) theory of colloidal forces (Kuroda et al., 2011; Soda et al., 2011), which was the most widely used framework for understanding colloidal stability considering the Van der Waals interaction, and the electric double layer interaction present between charged surfaces immersed in electrolyte solutions. Although at very short distances there were deviations that may be attributed to hydration forces or surface roughness (Ducker et al., 1991). This first attempt of interpretation of AFM force-distance curves in colloid system enhanced the study field of colloidal force measurement using AFM forward to explain and predict colloidal

phenomena in many applications.

In this chapter, surface forces were measured using AFM by approaching an elemental selenium sphere towards hydrophilic/hydrophobic surfaces. The aim of this work is to elucidate the surface interactions of elemental selenium and other solid particles that existing in aqueous solutions, and to reveal the surface forces governing the interactions.

4.2 Experimental

4.2.1 Materials

Selenium nanoparticles (primary size 100 nm, MK Impex Corp., Canada), silica particles (primary size 12 nm, Aldrich), glass slides (Fisher Scientific), sodium chloride (NaCl, ACS certified, Fisher Scientific), potassium chloride (KCl, ACS certified, Fisher Scientific), sodium hydroxide (NaOH, ACS certified, Fisher Scientific), hydrochloric acid (HCl, 1 N, ACS certified, Fisher Scientific), octadecyltrichlorosilane ($C_{18}H_{37}Cl_3Si$, 95%, ACROS Organics), chloroform ($CHCl_3$, ACS certified, Fisher Scientific), hexane (C_6H_{14}, ACS certified, Fisher Scientific), sodium selenite (Na_2SeO_3, anhydrous, ACROS Organics), and Lithium Chloride (LiCl, ⩾98.5%, Fisher Chemical), and ethanol (99.5%, anhydrous, ACROS Organics) were used as received. Muscovite mica sheets were purchased from S & J Trading Inc., Glen Oaks, NY. Silica wafers were prepared from nanoFAB, University of Alberta. Epoxy adhesive (EP41S-1HT) were purchased from Master Bond. All aqueous solutions were prepared using Milli-Q water (Millipore deionized, 18.2 MΩ·cm resistivity). Solution pH was adjusted using HCl and NaOH.

4.2.2 Preparation of surfaces

4.2.2.1 Silica

Silica wafer was cut into pieces of 2×2 cm^2. The pieces of silica wafer were cleaned by UV Ozone Cleaner (BioForce NanoScience) for 10 min, and then rinsed with Milli-Q water and dried with N_2.

4.2.2.2 OTS/silica

The silica wafer was chemically modified with octadecyltrichlorosilane (OTS) to generate a hydrophobic surface. The hydrophobization procedure was a modified method according to the literature (Headrick & Berrie, 2004). In detail, the cleaned silica wafer was immersed in solution of 2.0 mM OTS in 4:1 (v/v) hexane/chloroform solvent mixture for 24 h. Then the modified silica wafer was rinsed with chloroform and dried in air.

4.2.2.3 Au/mica

A layer of Au film was coated on freshly cleaved mica by using Electron Beam Physical Vapor Deposition (EBPVD) technique. The Au film was estimated to be 20-30 nm by controlling the deposition rate and time.

4.2.2.4 Se/Au/mica

Au/mica was rinsed with ethanol and Milli-Q water and dried with N_2. The cleaned Au/mica was used as working electrode and placed in 0.5 mM Na_2SeO_3 with 0.1 M LiCl as electrolyte. The solution pH was adjusted to 2, and saturated with N_2 for 20 min before use (Cabral, M. F.; Pedrosa, V. A.; Machado, S. A. S., 2010; Lai, Y., 2010). A Pt wire was used as a counter electrode and an Ag/AgCl (1 M KCl) electrode was used as a reference electrode (0.236 V vs SHE). All potentials quoted in this work were referred to this reference electrode, unless elsewise specified. The electrodeposition was performed at -

0.25 V for 600 s. The resulting working electrode was rinsed with Milli-Q water and dried with N_2.

4.2.3 Contact angle measurements

The sessile drop technique was used to measure contact angles of water on surfaces. A 3 μL aqueous droplet was placed onto surfaces through a microsyringe and contact angles were directly determined by the goniometer (ramé-hart instrument co.) software by analyzing the drop profile.

4.2.4 Zeta potential measurements

Zeta potential was measured using a Zetasizer Nano ZSP (Malvern Instruments, UK). Selenium particles were dispersed in 1 mM NaCl to a concentration of 1 mg L^{-1}. Silica particles were either directly dispersed in 1 mM NaCl, or modified with OTS according to the same procedure of preparing OTS/silica surfaces in 2.2.2 and then dispersed in 1 mM NaCl. The solution pH was adjusted by HCl and NaOH before measurements .

4.3 Results and discussion

4.3.1 Characterization of surfaces

Fig. 4.1a shows the Se film electrodeposited on Au coated mica surface (Se/Au/mica). The resulting Se film has a red color as compared to the gold-colored Au/mica. Fig. 4.1b shows a water droplet on the electrodeposited Se film showing a water contact angle of ~72°. The contact angle measured on OTS/silica is ~110° (picture not shown). Se/Au/mica

was characterized by Time-of-Flight Secondary Ion Mass Spectrometry, ToF-SIMS. The results shown in Fig. 4.2 indicate that Se was successfully deposited on the electrode.

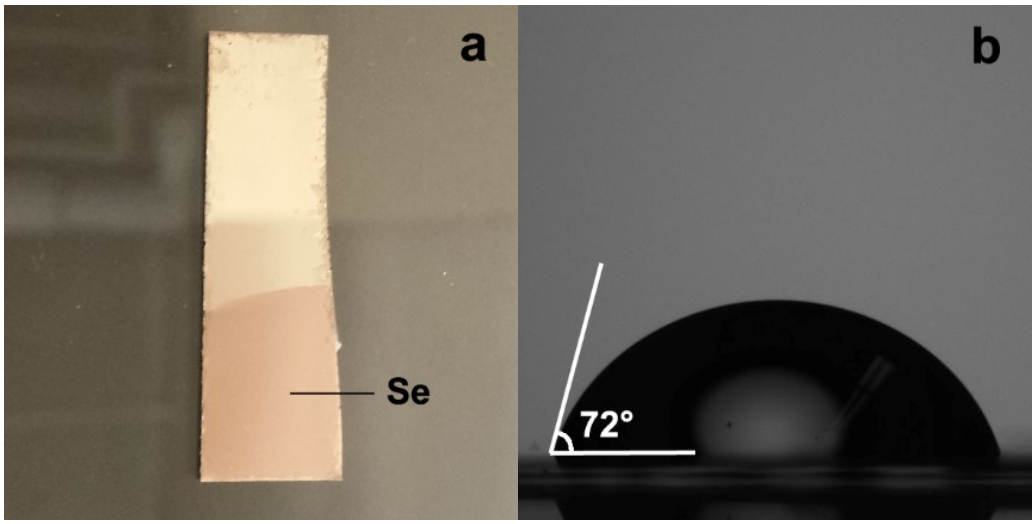

Figure 4.1. (a) Photography of Se film prepared by electrodeposition; (b) water drop on the prepared Se film showing a contact angle of ~72°

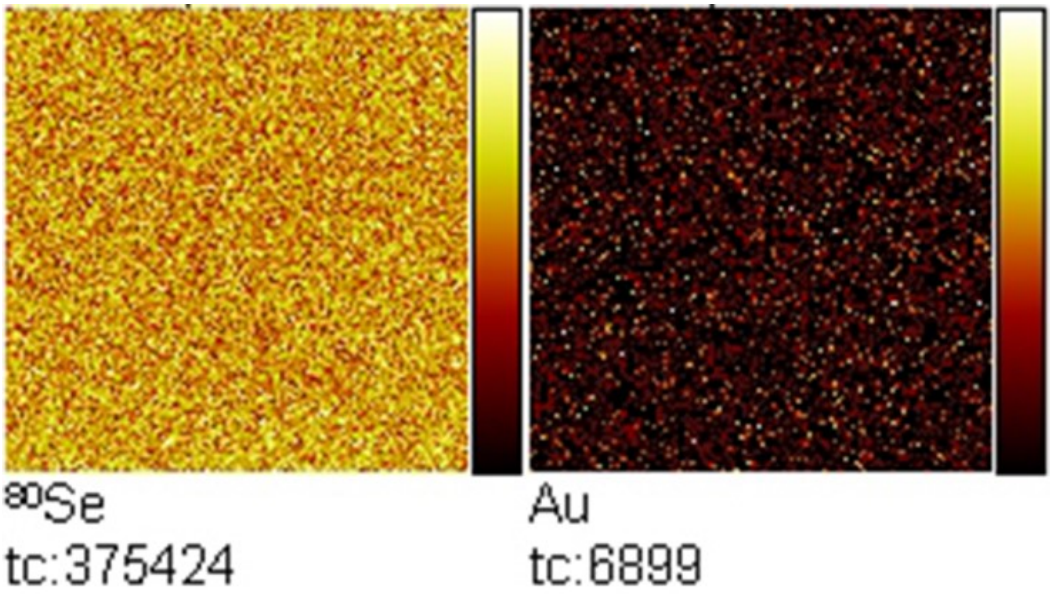

Figure 4.2. Time-of-Flight Secondary Ion Mass Spectrometry (ToF-SIMS) images of electrodeposited Se film

Fig. 4.3 shows the typical AFM topographic images of OTS/silica and electrodeposited Se film. The OTS modified surface (Fig. 4.3a) has a root-mean-squared roughness R_q of ~0.62 nm. The boundary region of Se film deposited on Au/mica was imaged (Fig. 4.3b). By measuring the height difference between the Se film (left region) and Au film (right region), the Se film thickness was estimated to be ~2 nm. The R_q of the Se film was obtained by imaging only the Se film region (Fig. 4.3c) as ~1.53 nm. The low surface roughness of OTS/silica and Se film facilitate the precise measurement of force curves between the Se probe and the prepared surfaces.

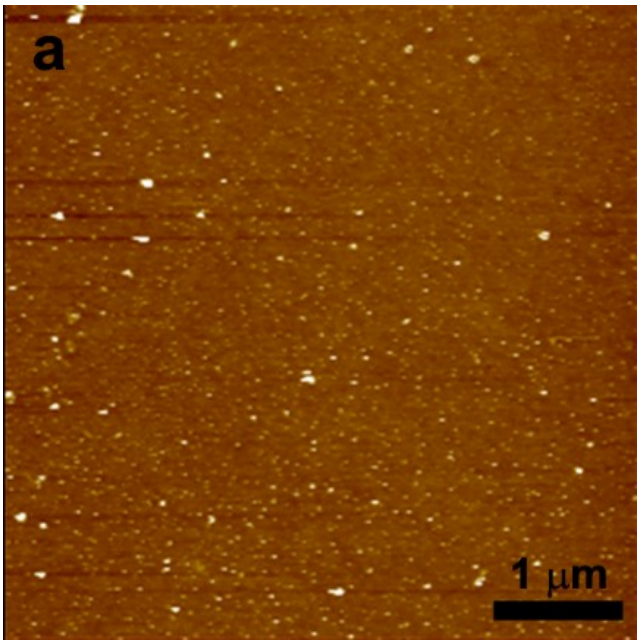

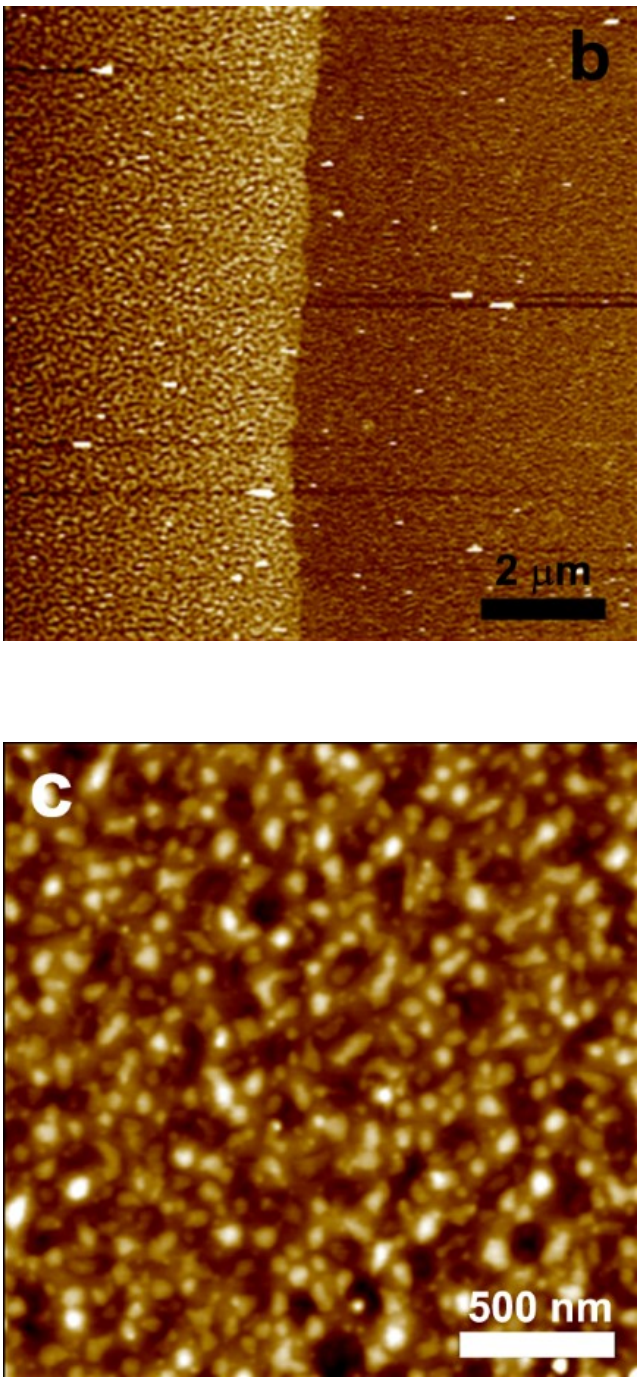

Figure 4.3. AFM topographic images of (a) OTS/silica; (b) boundary region of the electrodeposited Se film; (c) electrodeposited Se film

4.3.2 Interactions between Se sphere and solid surfaces

Fig. 4.4 shows the force curves measured by approaching a Se probe towards a silica

substrate in NaCl solutions. In 1 mM NaCl (Fig. 4.4a), long-range repulsive forces, which increases as increasing pH of the solution, and short range attractive forces are observed. The force curves can be theoretically predicted by Derjaguin-Landau-Verwey-Overbeek (DLVO) forces (F_{DLVO}), which consists of electric double layer forces (F_{edl}) and Van der Waals forces (F_{vdw}), and hydrodynamic forces (F_{hd}). A constant charge DLVO model was applied to by considering that a spherical Se probe was approaching an infinite flat substrate (Cappella & Dietler, 1999; J. N. Israelachvili, 2011):

$$F_{edl} = (\pi/\varepsilon\varepsilon_0\kappa^2)[(\sigma_T^2 + \sigma_S^2)(e^{-2\kappa R} + 2\kappa R - 1)e^{-2\kappa D} + 4\sigma_T\sigma_S(\kappa R + e^{-\kappa R} - 1)e^{-\kappa D}] \quad (4.1)$$

$$F_{vdw} = -A_{132}R / 6D^2 \quad (4.2)$$

where ε is the relative permittivity of medium, ε_0 the vacuum permittivity, κ the Debye length, σ_T the tip surface charge density, σ_S the substrate surface charge density, R the Se probe radius, D the separation distance between Se probe and flat substrate. Hamaker constants for media 1 and 2 interacting across medium 3, A_{132}, in this work are estimated according to Equation 3 (J. N. Israelachvili, 2011):

$$A_{132} \approx \sqrt{A_{131} \cdot A_{232}} \quad (4.3)$$

where A_{131} is for medium 1 interacting across medium 3 with itself, and A_{232} for medium 2 interacting across medium 3 with itself. Individual Hamaker constants used for calculations are summarized in Table 4.1. F_{hd} is described by Equation 4 (Tulpar & Walz, 2007):

$$F_{hd} = -6\pi\eta R^2 u / D, \text{ as } D/R \rightarrow 0 \quad (4.4)$$

where η is the fluid viscosity, and u the Se probe approaching velocity. In 0.5 M NaCl (Fig. 4.4b), the electric double layer is compressed, and no long-range repulsive forces are observed. The force curves are well characterized by F_{vdw} and F_{hd}.

Table 4.1. Hamaker constants used for calculations

Medium 1	Medium 3	Medium 2	A_{132} (10^{-20} J)
silica	H_2O	silica	0.46*
OTS	H_2O	OTS	0.50**
Se	H_2O	Se	5.82***

*Cappella and Dietler (1999)

**Ducker and Clarke (1994)

***Visser (1972)

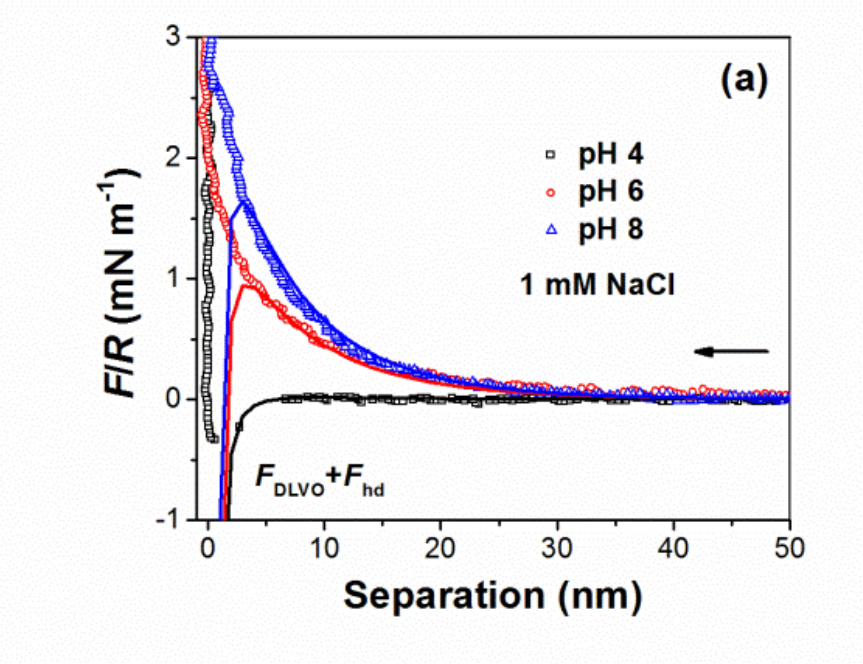

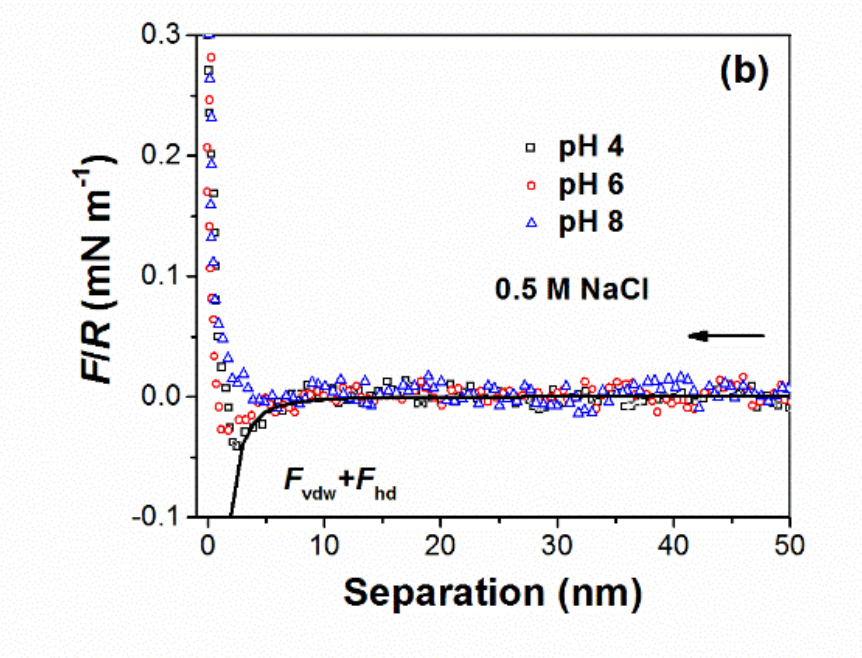

Figure 4.4. Force curves (plotted as normalized force F/R) measured by approaching a Se probe towards a silica substrate in (a) 1 mM NaCl; (b) 0.5 M NaCl. The hollow-dotted lines are experimental force curves. The solid lines are the theoretical calculations with $A = 1.64 \times 10^{-20}$ J; probe potential $\psi_T = -8$ mV, substrate potential $\psi_S = -3$ mV, at pH 4; $\psi_T = -35$ mV, $\psi_S = -25$ mV, at pH 6; $\psi_T = -35$ mV, $\psi_S = -38$ mV, at pH 8 (salt concentration is estimated to be 1.5 mM due to increased salinity during pH adjustment); η=0.001 N m^{-2} s (20℃) (D. R. Lide, 2005), $u = 1.98 \times 10^{-6}$ m s^{-1}.

Fig. 4.5 shows the force curves measured by approaching a selenium particle probe towards an OTS/silica substrate in NaCl solutions. In 1 mM NaCl (Fig. 4.5a), long-range repulsive F_{edl} are observed, which also increases as increasing pH of the solution. However, the force curves are not well predicted by only F_{DLVO} and F_{hd}, and an additional attractive force should be involved into the theoretical expression. Since the contact angles of Se film and OTS modified sureface were measured to be ~72° and ~110°, a hydrophobic force (F_{ho}) is expected to be responsible for the additional attraction interaction between the two surfaces, and is described by an exponential function given by Equation 4.5 (J. Israelachvili & Pashley, 1982)

$$F_{\mathrm{ho}}/R = C\mathrm{e}^{-D/D_0} \tag{4.5}$$

where C is the pre-exponential parameter, and D_0 the decay length of hydrophobic force. The forces curves are well predicted by F_{DLVO}, F_{ho}, and F_{hd}. In 0.5 M NaCl (Fig. 4.5b), the electric double layer is compressed, and the force curves can be well predicted by F_{vdw}, F_{ho}, and F_{hd}.

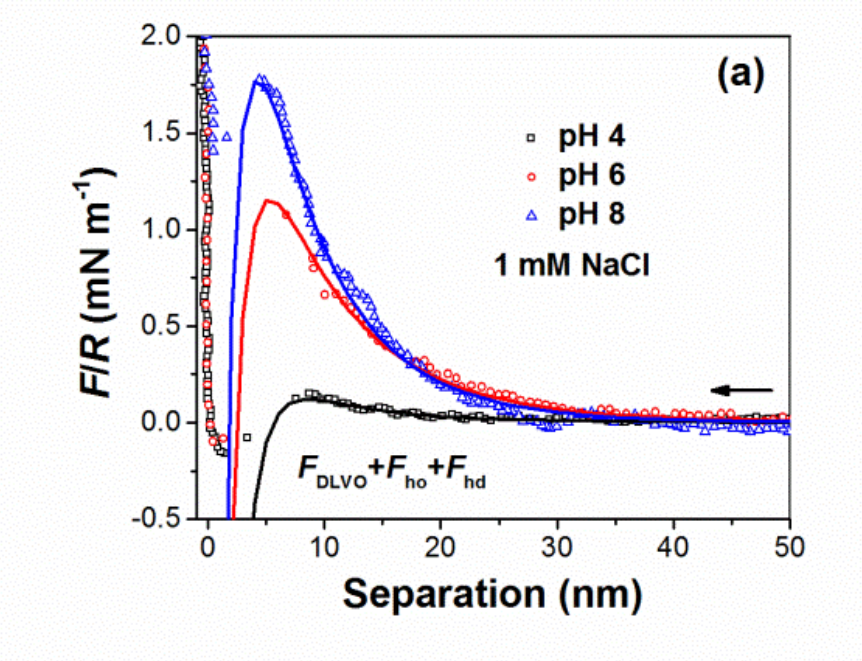

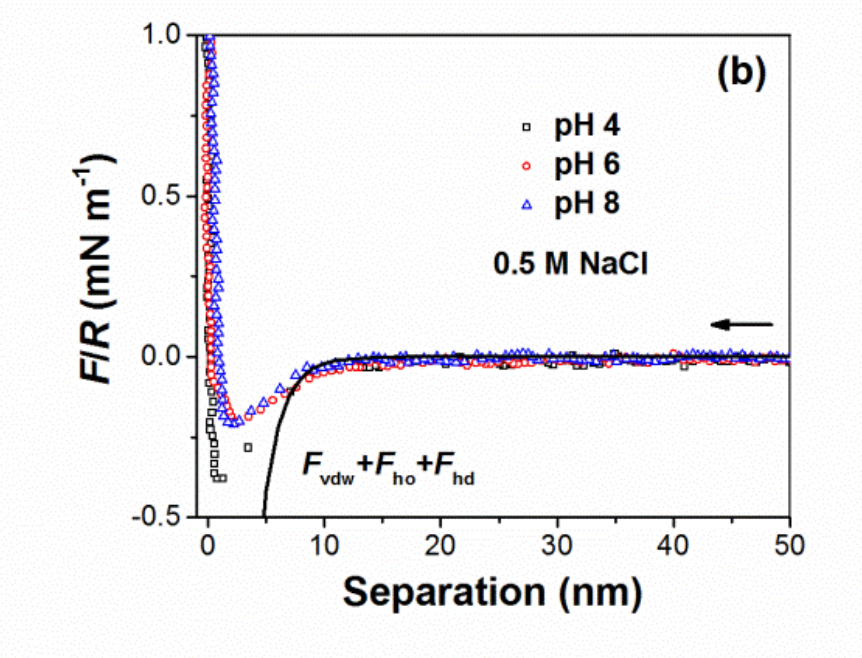

Figure 4.5. Force curves (plotted as normalized force F/R) measured by approaching a Se probe towards an OTS/silica substrate in (a) 1 mM NaCl; (b) 0.5 M NaCl. The hollow-dotted lines are experimental force curves. The solid lines are the theoretical calculations with $A = 1.70 \times 10^{-20}$ J; $\psi_T = -8$ mV, $\psi_S = -30$ mV, at pH 4; $\psi_T = -35$ mV, $\psi_S = -43$ mV, at pH 6; $\psi_T = -35$ mV, $\psi_S = -52$ mV, at pH 8 (salt concentration is estimated to be 1.5 mM due to increased salinity during pH adjustment); $\eta = 0.001$ N m^{-2} s (20℃),(D. R. Lide, 2005) $u = 1.98 \times 10^{-6}$ m s^{-1}; $C = 0.01$ N m^{-1}, $D_0 = 1.5$ nm.

Fig. 4.6 shows the force curves measured by approaching a Se probe towards a Se substrate in NaCl solutions. The force curves are similar to that of Se-OTS interactions as shown in Figure 4.5. However, it is found that F_{vdw} decays apparently faster than $1/D^2$ at D>10 nm. Considering the dielectric constants of silica (3.8) (J. N. Israelachvili, 2011), OTS (2.6) (Kulkarni, Kakade, Mulla, & Pillai, 2006), and Se (6) (Becker, Rademann, & Hensel, 1991), the dispersion energy for Se-Se interactions is considered suffering retardation effect. Therefore, the Hamaker constant of Se interacting across water is calculated using Equation 4.6 (the zero-frequency contribution remaining unchanged) (J. N. Israelachvili, 2011):

$$A \approx A_{\nu=0} + A_{\nu>0,\mathrm{Ret}} = A_{\nu=0} + A_{\nu>0,\mathrm{Non-ret}} / (1 + pD/100\mathrm{nm}) \quad (4.6)$$

where $A_{\nu=0}$ is the zero-frequency contribution, $A_{\nu>0,\mathrm{Ret}}$ the retarded dispersion contribution, $A_{\nu>0,\mathrm{Non\text{-}ret}}$ the nonretarded dispersion contribution, and p=14 for interactions between a sphere a planar surface. There is also a hydrophobic attraction between the Se probe and Se substrate, and the decay length of hydrophobic force (1 nm) is less than that of Se-OTS (1.5 nm), which suggests a weaker hydrophobic interactions of Se-Se compared to Se-OTS. The fitted surface potential (strictly the potential at stern plane of electric double layer) of Se film is more negative than that of Se sphere probe, which is possibly because of the different surface properties of Se prepared from different methods, e.g., the impact of Au underlayer.

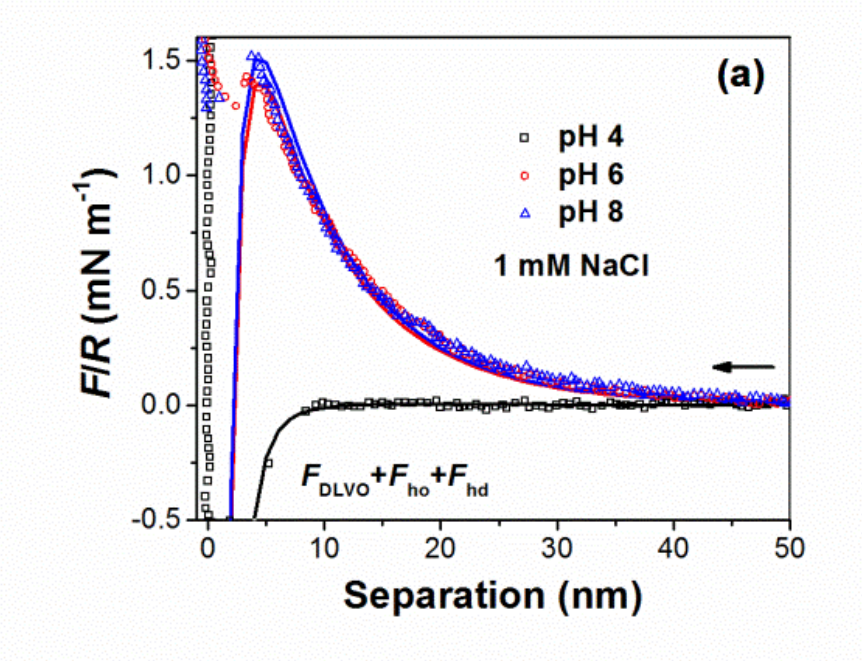

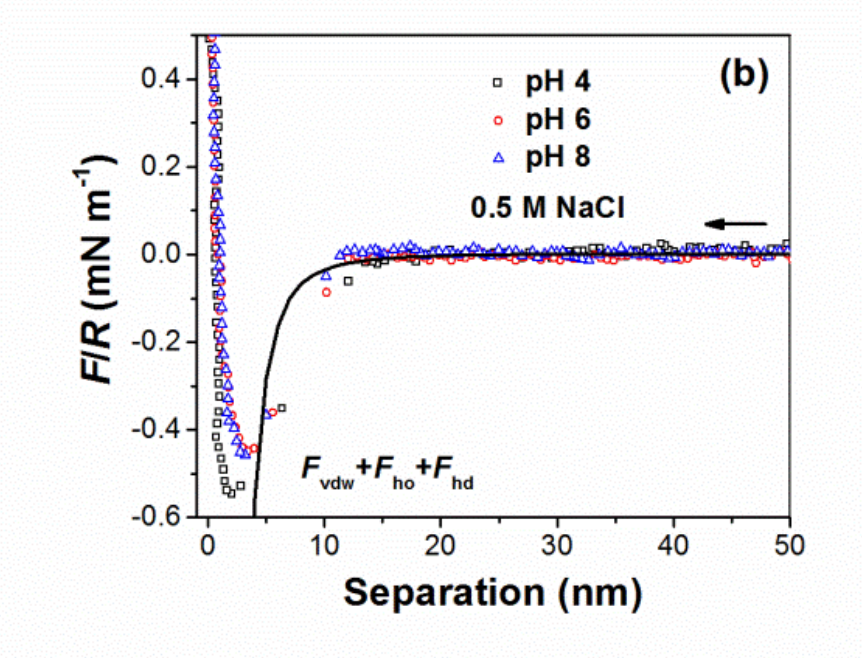

Figure 4.6. Force curves (plotted as normalized force F/R) measured by approaching a Se probe towards a Se substrate in (a) 1 mM NaCl (b) 0.5 M NaCl. The hollow-dotted lines are experimental force curves. The solid lines are the theoretical calculations with $A_{non\text{-}ret} = 5.82 \times 10^{-20}$ J; $\psi_T = \psi_S = -8$ mV, at pH 4; $\psi_T = -35$ mV, $\psi_S = -45$ mV, at pH 6; $\psi_T = -35$ mV, $\psi_S = -46$ mV, at pH 8; $\eta = 0.001$ N m^{-2} s (20℃),(David R. Lide, 2005) $u = 1.98 \times 10^{-6}$ m s^{-1}; $C = 0.01$ N m^{-1}, $D_0 = 1$ nm.

Fig. 4.7 shows the zeta potentials and surface potentials calculated from fitted AFM force curves of silica, OTS/silica, and Se probe. In general, with the increase of pH, the zeta potentials and AFM fitted potentials become more negative. Comparing the zeta potentials and fitted AFM surface potentials, the difference is not significant, and the AFM fitted surface potentials are slightly more negative than zeta potentials, except for OTS/silica, which shows larger error bars. This could be due to the nonuniform coating of OTS on silica surfaces.

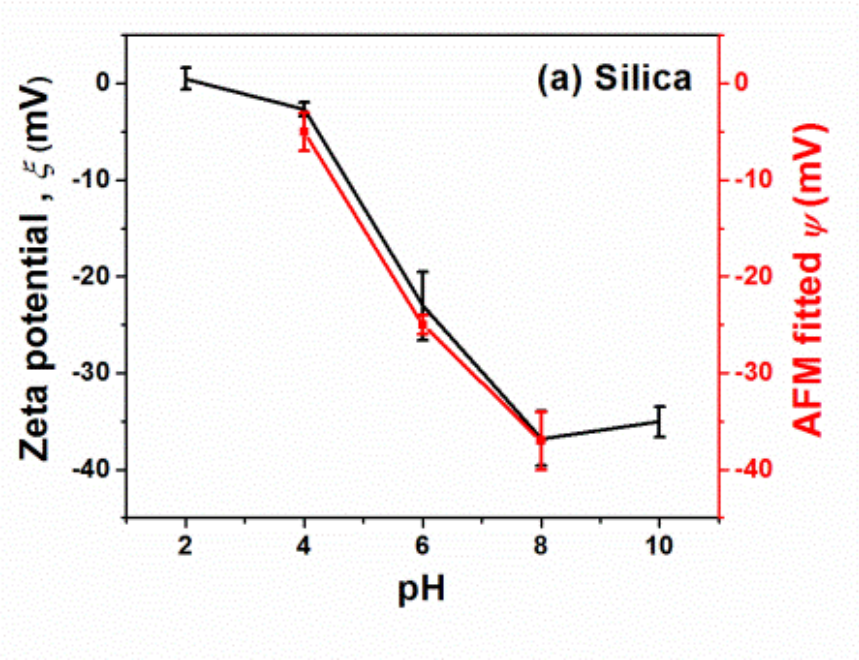
(a) Silica
Zeta potential , ζ (mV)
AFM fitted ψ (mV)
pH
0
-10
-20
-30
-40
2
4
6
8
10

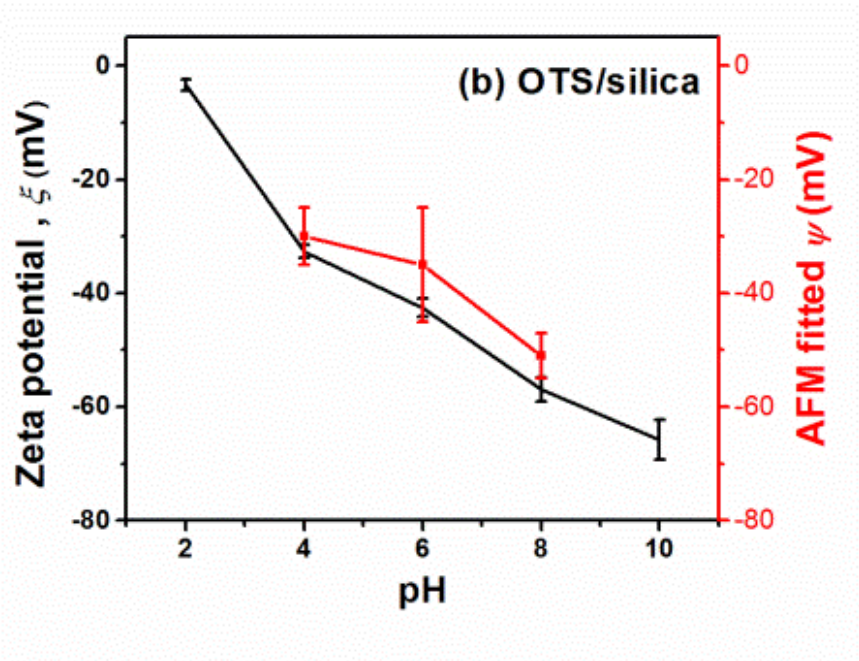
(b) OTS/silica
Zeta potential , ζ (mV)
AFM fitted ψ (mV)
pH
0
-20
-40
-60
-80
2
4
6
8
10

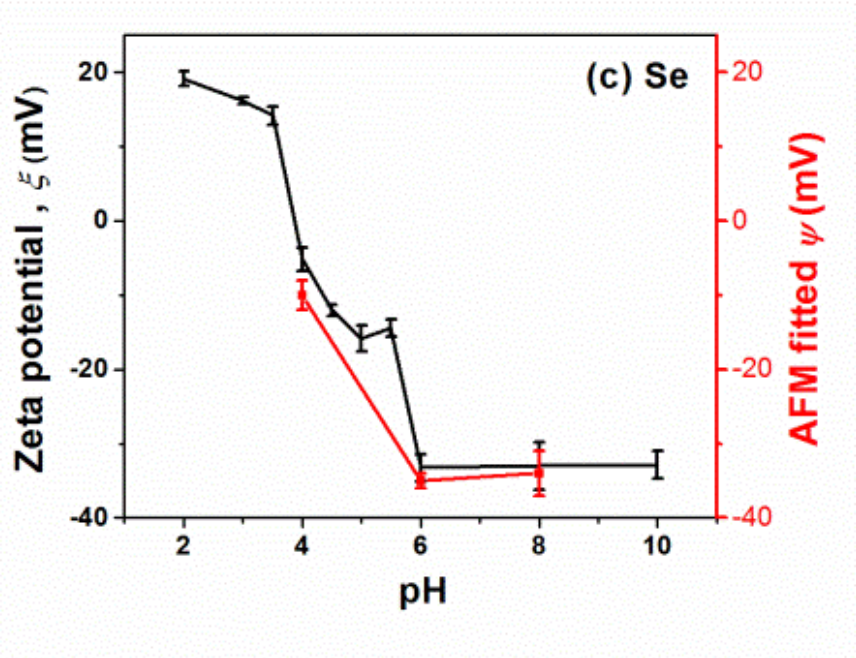

Figure 4.7. Comparison of measured zeta potentials (ξ) and surface potential (ψ) calculated from fitted AFM force curves. (a) silica, (b) OTS/silica, and (c) Se probe in 1 mM NaCl

Fig. 4.8 shows the summarized adhesion force (pull-off force) F_{ad} of Se-OTS modified silica, and Se-Se. Generally, F_{ad} decreases at relatively higher pH and lower salt concentration, and F_{ad} between Se and OTS is larger than that between Se and Se. If the measured F_{ad} is accounted for by Van der Waals interaction only, F_{ad} should not significantly change with pH and salt concentration by only considering interfacial energy γ_{132} (the subscript 1 refers to Se sphere, subscript 2 refers to OTS/silica or Se/Au/mica, and subscript 3 refers to aqueous solution), and F_{ad} of Se-OTS should be smaller than F_{ad} of Se-Se due to relatively smaller Hamaker constant of Se-H_2O-Se. Therefore, F_{ad} should be dominated by Van der Waals together with other forces, i.e., electrical force and hydrophobic force (Leckband & Israelachvili, 2001; Van Oss, 1993). The electrical force is either because of a non-real contact between two interacting surfaces, which is actually

a repulsive electric double layer interaction, or because of the accumulation of counterions close to the interacting solid surfaces (i.e., within stern layer)(Jönsson, Wennerstroem, & Halle, 1980), enhancing the final adhesion at lower pH and higher salt concentration (Leckband & Israelachvili, 2001). At the same ion concentration and pH, comparing F_{ad} of OTS-Se and Se-Se, the predominant force should be hydrophobic force, the only component that could result in larger F_{ad} of OTS-Se than Se-Se. This phenomenon can also be predicted by the water contact angles of OTS and Se, which suggests that the OTS film (~110°) is more hydrophobic than Se film (contact angle ~72°).

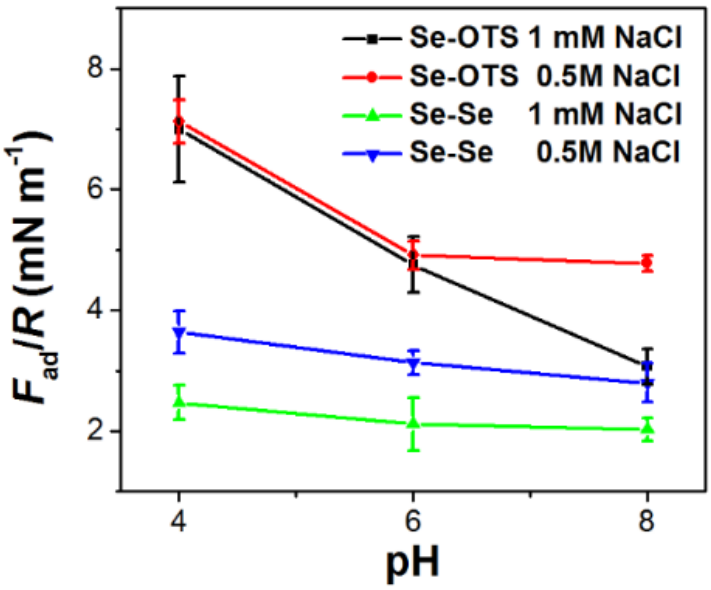

Figure 4.8. Summary of adhesion (pull-off) forces

4.4 Conclusions

Surface forces were directly measured using AFM by approaching an elemental Se sphere towards silica, OTS modified silica, and electrodeposited Se film surfaces in aqueous solutions. The surface interactions between Se and hydrophilic silica are dominated by DLVO forces in 1 mM NaCl. Increasing salt concentration in solution could compress the electric double layer, and Van der Waals forces appear to dominate. Hydrodynamic forces also significantly affect the interactions when the Se particle with considerable size is approaching the silica surface at a relatively high speed. The surface interactions between Se and hydrophobic surfaces (OTS/silica and Se/Au/mica) are dominated by DLVO forces and hydrophobic forces in 1 mM NaCl. The electric double layer is compressed in 0.5 M NaCl. The comparison of water contact angles of OTS and Se, and also the adhesion forces of Se-OTS and Se-Se, reveals that the hydrophobicity of Se is lower than OTS. The adhesion between Se and hydrophobic surface is enhanced at lower pH and higher salt concentration of solution, either because of a non-real contact between two interacting surfaces, which is actually a repulsive electric double layer interaction, or because of the accumulation of counterions close to the interacting solid surfaces. This work elucidates the surface interactions of elemental Se and hydrophilic/hydrophobic surfaces in aqueous solutions, and also reveals the surface forces governing the interactions, which are of both fundamental and applicable importance in processes where elemental Se is involved.

4.5 References

Becker, J., Rademann, K., & Hensel, F. (1991). Electronic structure of selenium-and tellurium-clusters. *Zeitschrift für Physik D Atoms, Molecules and Clusters, 19*(4), 233-235.

Buchs, B., Evangelou, M. W. H., Winkel, L. H. E., & Lenz, M. (2013). Colloidal properties of nanoparticular biogenic selenium govern environmental fate and bioremediation effectiveness. *Environmental science & technology, 47*(5), 2401-2407

Butt, H.-J. (1991). Measuring electrostatic, van der Waals, and hydration forces in electrolyte solutions with an atomic force microscope. *Biophysical Journal, 60*(6), 1438.

Cabral, M. F., Pedrosa, V. A., & Machado, S. A. S. (2010). Deposition of selenium thin layers on gold surfaces from sulphuric acid media: Studies using electrochemical quartz crystal microbalance, cyclic voltammetry and AFM. *Electrochimica Acta, 55*(3), 1184-1192

Cappella, B., & Dietler, G. (1999). Force-distance curves by atomic force microscopy. *Surface science reports, 34*(1), 1-104

Chaudhary, S., Umar, A., & Mehta, S. K. (2014). Surface functionalized selenium nanoparticles for biomedical applications. *Journal of biomedical nanotechnology, 10*(10), 3004-3042

Dagastine, R. R., Stevens, G. W., Chan, D. Y. C., & Grieser, F. (2004). Forces between two

oil drops in aqueous solution measured by AFM. *Journal of colloid and interface science, 273*(1), 339-342

Dowdle, P. R., & Oremland, R. S. (1998). Microbial oxidation of elemental selenium in soil slurries and bacterial cultures. *Environmental science & technology, 32*(23), 3749-3755.

Ducker, W. A., & Clarke, D. R. (1994). Controlled modification of silicon nitride interactions in water via zwitterionic surfactant adsorption. *Colloids and Surfaces A: Physicochemical and Engineering Aspects, 93*, 275-292

Ducker, W. A., Senden, T. J., & Pashley, R. M. (1991). Direct measurement of colloidal forces using an atomic force microscope.

Frisbie, C. D., Rozsnyai, L. F., Noy, A., Wrighton, M. S., & Lieber, C. M. (1994). Functional group imaging by chemical force microscopy. *Science, 265*(5181), 2071-2074

Headrick, J. E., & Berrie, C. L. (2004). Alternative method for fabricating chemically functionalized AFM tips: Silane modification of HF-treated Si3N4 probes. *Langmuir, 20*(10), 4124-4131.

Herbel, M. J., Blum, J. S., Oremland, R. S., & Borglin, S. E. (2003). Reduction of elemental selenium to selenide: experiments with anoxic sediments and bacteria that respire Se-oxyanions. *Geomicrobiology Journal, 20*(6), 587-602

Israelachvili, J., & Pashley, R. (1982). The hydrophobic interaction is long range, decaying

exponentially with distance.

Israelachvili, J. N. (2011). *Intermolecular and surface forces: revised third edition*: Academic press.

Jönsson, B., Wennerstroem, H., & Halle, B. (1980). Ion distributions in lamellar liquid crystals. A comparison between results from Monte Carlo simulations and solutions of the Poisson-Boltzmann equation. *The Journal of Physical Chemistry, 84*(17), 2179-2185

Kashiwa, M., Nishimoto, S., Takahashi, K., Ike, M., & Fujita, M. (2000). Factors affecting soluble selenium removal by a selenate-reducing bacterium Bacillus sp. SF-1. *Journal of bioscience and bioengineering, 89*(6), 528-533

Kessi, J., Ramuz, M., Wehrli, E., Spycher, M., & Bachofen, R. (1999). Reduction of Selenite and Detoxification of Elemental Selenium by the Phototrophic BacteriumRhodospirillum rubrum. *Applied and environmental microbiology, 65*(11), 4734-4740

Kulkarni, S. A., Kakade, B. A., Mulla, I. S., & Pillai, V. K. (2006). Suppression of electron-transfer characteristics of ferrocene by OTS monolayer on a silicon/electrolyte interface. *Journal of colloid and interface science, 299*(2), 777-784

Kuroda, M., Notaguchi, E., Sato, A., Yoshioka, M., Hasegawa, A., Kagami, T., . . . Soda, S. (2011). Characterization of Pseudomonas stutzeri NT-I capable of removing soluble selenium from the aqueous phase under aerobic conditions. *Journal of*

bioscience and bioengineering, 112(3), 259-264.

Lai, Y., Liu, F., Li, J., Zhang, Z., & Liu, Y. (2010). Nucleation and growth of selenium electrodeposition onto tin oxide electrode. *Journal of Electroanalytical Chemistry, 639*(1), 187-192

Lampis, S., Zonaro, E., Bertolini, C., Bernardi, P., Butler, C. S., & Vallini, G. (2014). Delayed formation of zero-valent selenium nanoparticles by Bacillus mycoides SeITE01 as a consequence of selenite reduction under aerobic conditions. *Microbial cell factories, 13*(1), 1-14

Leckband, D., & Israelachvili, J. (2001). Intermolecular forces in biology. *Quarterly reviews of biophysics, 34*(02), 105-267

Lide, D. R. (2005). CRC Handbook of Chemistry and Physics, (Internet Version 2008) CRC Press. *Boca Raton, FL*.

Losi, M. E., & Frankenberger, W. T. (1997). Reduction of selenium oxyanions by Enterobacter cloacae SLD1a-1: isolation and growth of the bacterium and its expulsion of selenium particles. *Applied and environmental microbiology, 63*(8), 3079-3084.

Ma, Y., Qi, L., Shen, W., & Ma, J. (2005). Selective synthesis of single-crystalline selenium nanobelts and nanowires in micellar solutions of nonionic surfactants. *Langmuir, 21*(14), 6161-6164

Narayanan, K. B., & Sakthivel, N. (2010). Biological synthesis of metal nanoparticles by

microbes. *Advances in colloid and interface science, 156*(1), 1-13

Oremland, R. S., Herbel, M. J., Blum, J. S., Langley, S., Beveridge, T. J., Ajayan, P. M., . . . Curran, S. (2004). Structural and spectral features of selenium nanospheres produced by Se-respiring bacteria. *Applied and environmental microbiology, 70*(1), 52-60

Rayman, M. P. (2000). The importance of selenium to human health. *The lancet, 356*(9225), 233-241

Soda, S., Kashiwa, M., Kagami, T., Kuroda, M., Yamashita, M., & Ike, M. (2011). Laboratory-scale bioreactors for soluble selenium removal from selenium refinery wastewater using anaerobic sludge. *Desalination, 279*(1), 433-438.

Staicu, L. C., van Hullebusch, E. D., Lens, P. N. L., Pilon-Smits, E. A. H., & Oturan, M. A. (2014). Electrocoagulation of colloidal biogenic selenium. *Environmental Science and Pollution Research, 22*(4), 3127-3137.

Steinberg, N. A., & Oremland, R. S. (1990). Dissimilatory selenate reduction potentials in a diversity of sediment types. *Applied and environmental microbiology, 56*(11), 3550-3557

Tulpar, A., & Walz, J. Y. (2007). Simultaneous measurement of structural and hydrodynamic forces between colloidal surfaces in complex fluids. *Colloids and Surfaces A: Physicochemical and Engineering Aspects, 300*(3), 268-280.

Vakarelski, I. U., Lee, J., Dagastine, R. R., Chan, D. Y. C., Stevens, G. W., & Grieser, F.

(2008). Bubble colloidal AFM probes formed from ultrasonically generated bubbles. *Langmuir, 24*(3), 603-605.

Van Oss, C. J. (1993). Acid—base interfacial interactions in aqueous media. *Colloids and Surfaces A: Physicochemical and Engineering Aspects, 78*, 1-49

Visser, J. (1972). On Hamaker constants: A comparison between Hamaker constants and Lifshitz-van der Waals constants. *Advances in colloid and interface science, 3*(4), 331-363

Wang, Q., & Webster, T. J. (2012). Nanostructured selenium for preventing biofilm formation on polycarbonate medical devices. *Journal of Biomedical Materials Research Part A, 100*(12), 3205-3210

Weisenhorn, A. L., Hansma, P. K., Albrecht, T. R., & Quate, C. F. (1989). Forces in atomic force microscopy in air and water. *Applied Physics Letters, 54*(26), 2651-2653

WHO, G. (2011). Guidelines for drinking-water quality. *World Health Organization*.

Zhang, Y., & Frankenberger, W. T. (2005). Removal of selenium from river water by a microbial community enhanced with Enterobacter taylorae in organic carbon coated sand columns. *Science of the Total Environment, 346*(1), 280-285

Zhang, Y., Zahir, Z. A., & Frankenberger, W. T. (2004). Fate of colloidal-particulate elemental selenium in aquatic systems. *Journal of environmental quality, 33*(2), 559-564

Chapter 5 Conclusions and Contributions

5.1 Conclusions

To understand the interactions between elemental selenium and different particles in wastewater, several techniques were applied in this work. The settling test was conducted to evaluate the selenium removal efficiency by using $Fe(OH)_3$ as coagulant. Zeta potential, QCM-D and AFM fore measurements were used to understand the coagulant adsorption mechanism and the interactions between selenium and different particles:

1) The elemental selenium nano particles were absorbed to amorphous $Fe(OH)_3$ in wastewater, governed by Van der Waals force as the electric double layers were compressed at high salt concentration.
2) $Fe(OH)_3$ had polymer-like behavior at the boundary layer, and the polymer behavior was promoted at low salt concentration.
3) For the best performance of $Fe(OH)_3$, the settling conditions were found to be around pH 8, since the amorphous $Fe(OH)_3$ had the most in content and more polymer behaved $Fe(OH)_3$ could 'trap' SeNPs, which enhanced the sweep flocculation behavior.
4) The surface interactions between Se and hydrophilic silica were dominated by DLVO forces in 1 mM NaCl. Increasing salt concentration in solution could compress the electric double layer, and Van der Waals forces appear to dominate.
5) Hydrodynamic forces also significantly affected the interactions when the Se particle with considerable size was approaching the silica surface at a relatively high speed.

6) The surface interactions between Se and hydrophobic surfaces (OTS/silica and Se/Au/mica) were dominated by DLVO forces and hydrophobic forces in 1 mM NaCl.
7) The electric double layer was compressed in 0.5 M NaCl. The comparison of water contact angles of OTS and Se, and also the adhesion forces of Se-OTS and Se-Se, revealed that the hydrophobicity of Se is lower than OTS.
8) The adhesion between Se and hydrophobic surface was enhanced at lower pH and higher salt concentration of solution, either because of a non-real contact between two interacting surfaces, which was actually a repulsive electric double layer interaction, or because of the accumulation of counterions closed to the interacting solid surfaces.

5.2 Contributions to the original knowledge

In this study, interaction between elemental selenium particles and different surfaces (i.e. $Fe(OH)_3$, silica, octadecyltrichlorosilane (OTS) and selenium film) were investigated to understand the behavior of elemental selenium particles during wastewater treatment process. The previous work mainly focus on the coagulant selection and performance condition on selenium nano particles removal. However, this study first time investigated the selenium nano particles behavior in wastewater at nano level by AFM and zeta potential measurement. The results had also provided better understanding of the coagulation process mechanism for treating selenium wastewater which is of both fundamentally and practically importance.

Chapter 6 Future Work

6.1 Settling experiments

In this study, $Fe(OH)_3$ coagulant was used for settling selenium particles. Other coagulants, such as aluminum salt and polymers, and flocculants are also applicable for wastewater treatment. Moreover, the industrial wastewater is complex with various dissolved solids and ions, each of which may have specific influence on the selenium removal performance. Therefore, simulated water with selected ions in laboratory is suggested to better understand the selenium removal mechanism in wastewater treatment.

1) As coagulants other than $Fe(OH)_3$, such as $Al(OH)_3$, are also efficient on removing colloidal impurities in wastewater, more settling tests could help compare the removal performance of coagulants and probably select a best coagulant for the removal of selenium particles.
2) Other than coagulant, flocculants such as polyacrylamide could enhance the coagulation process. Therefore, flocculants materials can be added after the quick mixing process in the settling test. Since selenium nano particles are negatively charged in wastewater, $Al(OH)_3$-polyacrylamide could be used with additional charge neutralizing effect.
3) The wastewater obtained from company has complex characteristics. The ions such as Ca^{2+} and Mg^{2+} could greatly impact the removal performance. Simulated water are need to investigate the ions impact on removal efficiency. Selenium nano particle are therefore needed to be generated in the laboratory.

6.2 AFM force measurements

Using AFM force measurement to determine the interactions between selenium particles and different surfaces can be further expanded by adding polymers and various salts.

1) As new coagulants introduced into the system, interactions between elemental selenium particles with coagulant surfaces such ($Al(OH)_3$ substrate) can be investigated by AFM force measurement.
2) Force measurement can also be done on the system involving polymers, which will help to understand the mechanism of coagulation and flocculation.
3) Different kinds of salts such as ($CaCl_2$ and $MgCl_2$) can be added to determine the ion effects on the forces acting in-between.

Bibliography

Balistrieri, L. S., & Chao, T. T. (1990). Adsorption of selenium by amorphous iron oxyhydroxide and manganese dioxide. *Geochimica et Cosmochimica Acta, 54*(3), 739-751

Becker, J., Rademann, K., & Hensel, F. (1991). Electronic structure of selenium-and tellurium-clusters. *Zeitschrift für Physik D Atoms, Molecules and Clusters, 19*(4), 233-235.

Behrens, S. H., & Borkovec, M. (1999). Electrostatic interaction of colloidal surfaces with variable charge. *The Journal of Physical Chemistry B, 103*(15), 2918-2928

Bitton, G. (2005). *Wastewater microbiology*: John Wiley & Sons.

Brown, K. M., & Arthur, J. R. (2001). Selenium, selenoproteins and human health: a review. *Public health nutrition, 4*(2b), 593-599

Buchs, B., Evangelou, M. W. H., Winkel, L. H. E., & Lenz, M. (2013). Colloidal properties of nanoparticular biogenic selenium govern environmental fate and bioremediation effectiveness. *Environmental science & technology, 47*(5), 2401-2407

Burau, R. G. (1985). Environmental chemistry of selenium. *California agriculture, 39*(7), 16-18

Butt, H.-J. (1991). Measuring electrostatic, van der Waals, and hydration forces in electrolyte solutions with an atomic force microscope. *Biophysical Journal, 60*(6), 1438.

Butt, H.-J., Cappella, B., & Kappl, M. (2005). Force measurements with the atomic force microscope: Technique, interpretation and applications. *Surface science reports, 59*(1).

Cappella, B., & Dietler, G. (1999). Force-distance curves by atomic force microscopy. *Surface science reports, 34*(1), 1-104

Chaudhary, S., Umar, A., & Mehta, S. K. (2014). Surface functionalized selenium nanoparticles for biomedical applications. *Journal of biomedical nanotechnology, 10*(10), 3004-3042

Chotas, H. G., Dobbins Iii, J. T., & Ravin, C. E. (1999). Principles of digital radiography with large-area, electronically readable detectors: a review of the basics. *Radiology, 210*(3), 595-599

Dagastine, R. R., Stevens, G. W., Chan, D. Y. C., & Grieser, F. (2004). Forces between two oil drops in aqueous solution measured by AFM. *Journal of colloid and interface science, 273*(1), 339-342

Dowdle, P. R., & Oremland, R. S. (1998). Microbial oxidation of elemental selenium in soil slurries and bacterial cultures. *Environmental science & technology, 32*(23), 3749-3755.

Duan, J., & Gregory, J. (2003). Coagulation by hydrolysing metal salts. *Advances in colloid and interface science, 100*, 475-502

Ducker, W. A., & Clarke, D. R. (1994). Controlled modification of silicon nitride interactions in water via zwitterionic surfactant adsorption. *Colloids and Surfaces A: Physicochemical and Engineering Aspects, 93*, 275-292

Ducker, W. A., Senden, T. J., & Pashley, R. M. (1991). Direct measurement of colloidal forces using an atomic force microscope.

Dungan, R. S., & Frankenberger, W. T. (1999). Microbial transformations of selenium and the bioremediation of seleniferous environments. *Bioremediation Journal, 3*(3), 171-188.

Eckenfelder Jr, W. W. (2000). Industrial Water Pollution Control: Mc Graw Hill Book Company, New York.

Fitzpatrick, C. (2013). Envirogen awarded patent for fluidized bed reactor treatment of perchlorate contaminated water.

Foster, L. H., & Sumar, S. (1997). Selenium in health and disease: a review. *Critical Reviews in Food Science & Nutrition, 37*(3), 211-228

Frankenberger Jr, W. T., & Karlson, U. (1994). Microbial volatilization of selenium from soils and sediments. *Selenium in the Environment*, 369-387.

Frankenberger, W. T., & Engberg, R. A. (1998). *Environmental chemistry of selenium*: CRC Press.

Frisbie, C. D., Rozsnyai, L. F., Noy, A., Wrighton, M. S., & Lieber, C. M. (1994). Functional group imaging by chemical force microscopy. *Science, 265*(5181), 2071-2074

Fritzmann, C., Löwenberg, J., Wintgens, T., & Melin, T. (2007). State-of-the-art of reverse osmosis desalination. *Desalination, 216*(1), 1-76

Fu, Y. (2014). *Water-Dispersible Magnetic Particle-Graphene Oxide Composites: Synthesis, Characterization and Application in the Removal of Selenium Oxyanions.* University of Alberta.

Hamilton, S. J. (2004). Review of selenium toxicity in the aquatic food chain. *Science of the Total Environment, 326*(1), 1-31

Hatzinger, P. B., Greene, M. R., Frisch, S., Togna, A. P., Manning, J., & Guarini, W. J. (2000). Biological treatment of perchlorate-contaminated groundwater using fluidized bed reactors *Case studies in the remediation of chlorinated and recalcitrant compounds* (pp. 115-122): Citeseer.

Haygarth, P. M. (1994). Global importance and global cycling of selenium. *Selenium in the Environment*, 1-27.

Headrick, J. E., & Berrie, C. L. (2004). Alternative method for fabricating chemically functionalized AFM tips: Silane modification of HF-treated Si3N4 probes. *Langmuir, 20*(10), 4124-4131.

Herbel, M. J., Blum, J. S., Oremland, R. S., & Borglin, S. E. (2003). Reduction of elemental selenium to selenide: experiments with anoxic sediments and bacteria that respire Se-oxyanions. *Geomicrobiology Journal, 20*(6), 587-602

Hill, C. M. (2010). Review of Available Technologies for the Removal of Selenium from Water. *Final Report, prepared for North American Metals Council (NAMC)*.

Instruments, M. (2011). Zeta potential: An Introduction in 30 minutes. *Zetasizer Nano Serles Technical Note. MRK654-01*.

Israelachvili, J., & Pashley, R. (1982). The hydrophobic interaction is long range, decaying exponentially with distance.

Israelachvili, J. N. (2011). *Intermolecular and surface forces: revised third edition*: Academic press.

Jönsson, B., Wennerstroem, H., & Halle, B. (1980). Ion distributions in lamellar liquid crystals. A comparison between results from Monte Carlo simulations and solutions

of the Poisson-Boltzmann equation. *The Journal of Physical Chemistry, 84*(17), 2179-2185

Johnson, P. N., & Amirtharajah, A. (1983). Ferric chloride and alum as single and dual coagulants. *Journal (American Water Works Association)*, 232-239

Kapoor, A., Tanjore, S., & Viraraghavan, T. (1995). Removal of selenium from water and wastewater. *International journal of environmental studies, 49*(2), 137-147

Kashiwa, M., Nishimoto, S., Takahashi, K., Ike, M., & Fujita, M. (2000). Factors affecting soluble selenium removal by a selenate-reducing bacterium Bacillus sp. SF-1. *Journal of bioscience and bioengineering, 89*(6), 528-533

Kessi, J., Ramuz, M., Wehrli, E., Spycher, M., & Bachofen, R. (1999). Reduction of Selenite and Detoxification of Elemental Selenium by the Phototrophic BacteriumRhodospirillum rubrum. *Applied and environmental microbiology, 65*(11), 4734-4740

Kulkarni, S. A., Kakade, B. A., Mulla, I. S., & Pillai, V. K. (2006). Suppression of electron-transfer characteristics of ferrocene by OTS monolayer on a silicon/electrolyte interface. *Journal of colloid and interface science, 299*(2), 777-784

Kuroda, M., Notaguchi, E., Sato, A., Yoshioka, M., Hasegawa, A., Kagami, T., . . . Soda, S. (2011). Characterization of Pseudomonas stutzeri NT-I capable of removing soluble selenium from the aqueous phase under aerobic conditions. *Journal of bioscience and bioengineering, 112*(3), 259-264.

Lampis, S., Zonaro, E., Bertolini, C., Bernardi, P., Butler, C. S., & Vallini, G. (2014). Delayed formation of zero-valent selenium nanoparticles by Bacillus mycoides

SeITE01 as a consequence of selenite reduction under aerobic conditions. *Microbial cell factories, 13*(1), 1-14

Leckband, D., & Israelachvili, J. (2001). Intermolecular forces in biology. *Quarterly reviews of biophysics, 34*(02), 105-267

Lemly, A. D. (2004). Aquatic selenium pollution is a global environmental safety issue. *Ecotoxicology and environmental safety, 59*(1), 44-56

Li, T., Zhu, Z., Wang, D., Yao, C., & Tang, H. (2006). Characterization of floc size, strength and structure under various coagulation mechanisms. *Powder technology, 168*(2), 104-110

Lide, D. R. (2005). *CRC handbook of chemistry and physics* (Internet Version 2005 ed.). Boca Raton, FL: CRC Press.

Lide, D. R. (2005). CRC Handbook of Chemistry and Physics, (Internet Version 2008) CRC Press. *Boca Raton, FL*.

Losi, M. E., & Frankenberger, W. T. (1997). Reduction of selenium oxyanions by Enterobacter cloacae SLD1a-1: isolation and growth of the bacterium and its expulsion of selenium particles. *Applied and environmental microbiology, 63*(8), 3079-3084.

Ma, Y., Qi, L., Shen, W., & Ma, J. (2005). Selective synthesis of single-crystalline selenium nanobelts and nanowires in micellar solutions of nonionic surfactants. *Langmuir, 21*(14), 6161-6164

Manual, Z. N. S. U. (2003). Malvern Instruments Ltd. *Manual Version IM, 100*, 1.23-21.26.

Meyer, E. E., Rosenberg, K. J., & Israelachvili, J. (2006). Recent progress in understanding hydrophobic interactions. *Proceedings of the National Academy of Sciences, 103*(43), 15739-15746.

Munirathinam, K., Srinivasan, R., Tudini, J. J., Sandy, T. A., & Harrison, T. D. (2011). Selenium treatment of mine water effluent in a fluidized bed reactor (FBR). *Proceedings of the Water Environment Federation, 2011*(18), 157-177

Narayanan, K. B., & Sakthivel, N. (2010). Biological synthesis of metal nanoparticles by microbes. *Advances in colloid and interface science, 156*(1), 1-13

Navarro-Alarcon, M., & Cabrera-Vique, C. (2008). Selenium in food and the human body: a review. *Science of the Total Environment, 400*(1), 115-141

Oberhauser, A. F., Marszalek, P. E., Erickson, H. P., & Fernandez, J. M. (1998). The molecular elasticity of the extracellular matrix protein tenascin. *Nature, 393*(6681), 181-185

Oremland, R. S., Herbel, M. J., Blum, J. S., Langley, S., Beveridge, T. J., Ajayan, P. M., . . . Curran, S. (2004). Structural and spectral features of selenium nanospheres produced by Se-respiring bacteria. *Applied and environmental microbiology, 70*(1), 52-60

Rabinovich, Y. I., & Yoon, R. H. (1994). Use of atomic force microscope for the measurements of hydrophobic forces. *Colloids and Surfaces A: Physicochemical and Engineering Aspects, 93*, 263-273

Rayman, M. P. (2000). The importance of selenium to human health. *The lancet, 356*(9225), 233-241

Reid, M. E., Stratton, M. S., Lillico, A. J., Fakih, M., Natarajan, R., Clark, L. C., & Marshall, J. R. (2004). A report of high-dose selenium supplementation: response and toxicities. *Journal of Trace Elements in Medicine and Biology, 18*(1), 69-74

Revil, A., Pezard, P. A., & Glover, P. W. J. (1999). Streaming potential in porous media: 1. Theory of the zeta potential. *Journal of Geophysical Research: Solid Earth (1978–2012), 104*(B9), 20021-20031.

Rief, M., Gautel, M., Oesterhelt, F., Fernandez, J. M., & Gaub, H. E. (1997). Reversible unfolding of individual titin immunoglobulin domains by AFM. *Science, 276*(5315), 1109-1112.

Rotruck, J. T., Pope, A. L., Ganther, H. E., Swanson, A. B., Hafeman, D. G., & Hoekstra, W. G. (1973). Selenium: biochemical role as a component of glutathione peroxidase. *Science, 179*(4073), 588-590.

Sandy, T., & DiSante, C. (2010). Review of available technologies for the removal of selenium from water. *North Amerian metals council*.

Sauerbrey, G. (1959). Verwendung von Schwingquarzen zur Wägung dünner Schichten und zur Mikrowägung. *Zeitschrift für physik, 155*(2), 206-222

Schott, H. (1981). Electrokinetic studies of magnesium hydroxide. *Journal of pharmaceutical sciences, 70*(5), 486-489

Semerjian, L., & Ayoub, G. M. (2003). High-pH–magnesium coagulation–flocculation in wastewater treatment. *Advances in Environmental Research, 7*(2), 389-403.

Shammas, N. K. (2005). Coagulation and flocculation *Physicochemical treatment processes* (pp. 103-139): Springer.

Smith, A. M., & Nie, S. (2009). Semiconductor nanocrystals: structure, properties, and band gap engineering. *Accounts of chemical research, 43*(2), 190-200

Sobolewski, A. (2005). Evaluation of treatment options to reduce water-borne selenium at coal mines in west-central Alberta. *Report, Microbial Technologies Inc, 2006*, 32.

Soda, S., Kashiwa, M., Kagami, T., Kuroda, M., Yamashita, M., & Ike, M. (2011). Laboratory-scale bioreactors for soluble selenium removal from selenium refinery wastewater using anaerobic sludge. *Desalination, 279*(1), 433-438.

Sonstegard, J., Pickett, T., Harwood, J., & Johnson, D. (2008). Full scale operation of GE ABMet® biological technology for the removal of selenium from FGD wastewaters. *IWC, 8*, 31.

Staicu, L. C., van Hullebusch, E. D., Lens, P. N. L., Pilon-Smits, E. A. H., & Oturan, M. A. (2014). Electrocoagulation of colloidal biogenic selenium. *Environmental Science and Pollution Research, 22*(4), 3127-3137.

Staicu, L. C., Van Hullebusch, E. D., Oturan, M. A., Ackerson, C. J., & Lens, P. N. L. (2015). Removal of colloidal biogenic selenium from wastewater. *Chemosphere, 125*, 130-138

Steinberg, N. A., & Oremland, R. S. (1990). Dissimilatory selenate reduction potentials in a diversity of sediment types. *Applied and environmental microbiology, 56*(11), 3550-3557

Tulpar, A., & Walz, J. Y. (2007). Simultaneous measurement of structural and hydrodynamic forces between colloidal surfaces in complex fluids. *Colloids and Surfaces A: Physicochemical and Engineering Aspects, 300*(3), 268-280.

Twidwell, L. G., McCloskey, J., Miranda, P., & Gale, M. (2000). Technologies and potential technologies for removing selenium from process and mine wastewater. *Proc, Minor Elements, Soc of Mining Engineers, Salt Lake City*, 53-66.

Vakarelski, I. U., Lee, J., Dagastine, R. R., Chan, D. Y. C., Stevens, G. W., & Grieser, F. (2008). Bubble colloidal AFM probes formed from ultrasonically generated bubbles. *Langmuir, 24*(3), 603-605.

Valtiner, M., Kristiansen, K., Greene, G. W., & Israelachvili, J. N. (2011). Effect of surface roughness and electrostatic surface potentials on forces between dissimilar surfaces in aqueous solution. *Advanced materials, 23*(20), 2294-2299

Van Oss, C. J. (1993). Acid—base interfacial interactions in aqueous media. *Colloids and Surfaces A: Physicochemical and Engineering Aspects, 78*, 1-49

Visser, J. (1972). On Hamaker constants: A comparison between Hamaker constants and Lifshitz-van der Waals constants. *Advances in colloid and interface science, 3*(4), 331-363

Wang, H., Zhang, J., & Yu, H. (2007). Elemental selenium at nano size possesses lower toxicity without compromising the fundamental effect on selenoenzymes: comparison with selenomethionine in mice. *Free Radical Biology and Medicine, 42*(10), 1524-1533

Wang, N., Hsu, C., Zhu, L., Tseng, S., & Hsu, J.-P. (2013). Influence of metal oxide nanoparticles concentration on their zeta potential. *Journal of colloid and interface science, 407*, 22-28

Wang, Q., & Webster, T. J. (2012). Nanostructured selenium for preventing biofilm formation on polycarbonate medical devices. *Journal of Biomedical Materials Research Part A, 100*(12), 3205-3210

Webster, T. S., Guarini, W. J., & Wong, H. S. (2009). Fluidized bed bioreactor treatment of perchlorate-laden groundwater to potable standards. *J. American Water Works Association, 101*, 137-151.

Weisenhorn, A. L., Hansma, P. K., Albrecht, T. R., & Quate, C. F. (1989). Forces in atomic force microscopy in air and water. *Applied Physics Letters, 54*(26), 2651-2653

WHO, G. (2011). Guidelines for drinking-water quality. *World Health Organization*.

Wilber, C. G. (1980). Toxicology of selenium: a review. *Clinical toxicology, 17*(2), 171-230

Zhang, Y., & Frankenberger, W. T. (2005). Removal of selenium from river water by a microbial community enhanced with Enterobacter taylorae in organic carbon coated sand columns. *Science of the Total Environment, 346*(1), 280-285

Zhang, Y., Wang, J., Amrhein, C., & Frankenberger, W. T. (2005). Removal of selenate from water by zerovalent iron. *Journal of environmental quality, 34*(2), 487-495

Zhang, Y., Zahir, Z. A., & Frankenberger, W. T. (2004). Fate of colloidal-particulate elemental selenium in aquatic systems. *Journal of environmental quality, 33*(2), 559-564